Energy Conversion and Management 346 (2025) 120441

Contents lists available at ScienceDirect

Energy Conversion and Management

journal homepage: www.elsevier.com/locate/enconman

Research Paper

Multi-dish configurations for single-shaft and parallel-flow solar-dish Brayton cycles

C.C. Cockcroft, W.G. Le Roux *

Department of Mechanical and Aeronautical Engineering, University of Pretoria, Private Bag X20, Hatfield, Pretoria 0028, South Africa

ARTICLE INFO

Keywords:
Brayton cycle
Gas turbine
Turbocharger
Concentrating solar power
Recuperation

ABSTRACT

Concentrating solar power combined with parallel-flow Brayton cycles can form a viable solution to generating cleaner and more sustainable energy. Parallel-flow Brayton cycles are not influenced as greatly as traditional single-shaft cycles when solar and/or recuperation components are added to the cycle. To further improve the thermal efficiency of parallel-flow cycles, the solar heat input to the cycles can be increased through introducing a second solar receiver in the setup (a multi-dish setup). This analytical study addresses the viability of incorporating multi-dish configurations in parallel-flow and single-shaft Brayton cycles. The study is based on using off-the-shelf automotive turbochargers to develop a solarised micro gas turbine for power generation. It is determined that a multi-dish cycle setup adds performance improvement to the thermal efficiency results in both single-shaft and parallel-flow recuperated solar cycles. When the best-performing multi-dish recuperated low-temperature turbine (LTT) cycle is considered, the thermal efficiency is 69 % greater than in the best-performing single-dish recuperated LTT cycle. The multi-dish recuperated single-shaft cycle, however, obtains 3.2 % less thermal efficiency than the single-dish recuperated single-shaft cycle. The multi-dish single-shaft power output is greatly restricted by high solar receiver surface temperatures, which is not the case in the multi-dish recuperated LTT cycle. Therefore, more solar heat can be captured in the parallel-flow multi-dish LTT cycle.

1. Introduction

The utilisation of waste heat energy is a valuable form of clean energy [1]. A regenerative Brayton cycle, where waste heat is used to add heat to the cycle, is often used in gas turbine electricity generation [2] due to low maintenance and operational costs [3]. Besides the use of regeneration in a Brayton cycle (through using a recuperator), solar hybridisation, to form a concentrated solar power (CSP) Brayton cycle power generation plant further reduces the cycle running costs (by allowing for fuel savings) and improves the thermal efficiency of the cycle [4]. The overall thermal efficiency is shown to be between 35.8 % and 37.3 %, depending on the location of application, for an overall well-performing 4.6 MW central tower system coupled to a Brayton cycle, as analysed by Ref. [4]. Recent developments in solarised Brayton cycles, such as the cascade S-CO_2 cycle proposed by Ref. [5], further demonstrate the growing interest in hybrid CSP configurations optimised for both thermal efficiency and economic feasibility.

The first full-scale CSP Brayton cycle power plant was developed and demonstrated by Garret AiResearch and Sanders Associates from 1982 to 1984 [6,7,8]. This recuperated power plant was able to generate a power output of 0.4 kWe using a 44 m^2 solar dish in a sun-only test. However, when this power plant setup used a bigger solar dish with a dish area of 49 m^2 and with the supplementation of cycle heat through the use of the injection of methane gas into the cycle to form a hybrid power plant, the cycle was able to generate up to 2.9 kWe of power. Further development of a solar-dish Brayton cycle has been done in the form of the OMSoP project between 2013 and 2017 [9]. This study has initially been shown to have a peak theoretical system total thermal efficiency of approximately 25.8 %. A model, that has not been experimentally developed as of yet, has been analytically developed to optimise the OMSoP cycle efficiency with a targeted average thermal efficiency of 21 % with a potential 10 kWe of power output [10]. In 2011 the SolarCAT CSP Brayton cycle project was also developed but this project has not undergone further development besides that of initial sub-assembly testing [11]. Additional CSP Brayton cycle concepts have been studied in a closed loop form with supercritical carbon dioxide being used as the working fluid. This has been done in the study by Sammoutos et al. [12], where it has been shown that a solar Brayton cycle (with supercritical carbon dioxide) is capable of achieving a thermodynamic efficiency of 34.2 % without recuperation and up to 42.9 % with recuperation. This is for a large-scale system with a

* Corresponding author.
E-mail address: willem.leroux@up.ac.za (W.G. Le Roux).

https://doi.org/10.1016/j.enconman.2025.120441
Received 31 December 2024; Received in revised form 5 August 2025; Accepted 25 August 2025
Available online 18 September 2025
0196-8904/© 2025 The Authors. Published by Elsevier Ltd. This is an open access article under the CC BY-NC license (http://creativecommons.org/licenses/by-nc/4.0/).

Nomenclature

Symbols

A	Area [m^2]
AFR	Air-fuel ratio [-]
a	Recuperator channel width [m]
b	Recuperator channel height [m]
F	View factor
k	Thermal conductivity [W/mK]
L	Length [m]
M	Molecular mass [kg/mol]
$\dot{m}$	Mass flow rate [kg/s]
N	Number of tube sections
$\dot{n}$	Molar flow rate [mol/s]
n	Number of recuperator channels in a single direction [-]
P	Pressure [Pa]
$\dot{Q}$	Heat transfer rate [W]
r	Pressure ratio [-]
T	Temperature [K]
t	Thickness [m]
$\dot{W}$	Rate of work [W]

Greek symbols

ε	Emissivity
η	Efficiency
λ	Heat transfer coefficient [W/m^2K]
σ	Stefan-Boltzmann constant [W/m^2K]

Subscripts

0	Ambient
1–9	States 1–9
air	Air
CC	Combustion chamber
comp	Compressor
gt	Gasifier turbine
ins	Insulation
LPG	Liquified petroleum gas
mass	On a mass basis
max	Maximum
mole	On a mole basis
n	Tube section number
net	Net amount
pt	Power turbine
rec	Recuperator
s	Surface
SR	Solar receiver
th	Thermal

Superscripts

*	Solar

Abbreviations

AR	Aspect Ratio
CC	Combustion Chamber
CSP	Concentrating Solar Power
DNI	Direct Normal Irradiance
G	Generator
GT	Gasifier Turbine
HTT	High-Temperature Turbine
ITT	Intermediate-Temperature Turbine
ITT(S)	Intermediate-Temperature Turbine (Solarised)
LPG	Liquefied Petroleum Gas
LTT	Low-Temperature Turbine
NTU	Number of Transfer Units
OMSoP	European Optimised Microturbine Solar Power system
PT	Power Turbine
SR	Solar Receiver
SR-CC	Solar receiver placement 1 (before the CC)
SR-PT	Solar receiver placement 2 (before the PT)
SS	Single-Shaft
ST-CHP	Solar Turbo-Combined Heat and Power

maximum power output of 4.08 MW.

Researchers at the University of Pretoria, have also done extensive research into developing a small-scale CSP dish-Brayton power plant, through utilising entropy generation minimisation to optimise the geometry of the solar receiver and the recuperator [13,14] and through expanding the power plant into a hybrid plant that functions through the injection of liquified petroleum gas (LPG) [15]. In addition to this, cycle improvements have been considered through utilising integrated solar receiver phase-change materials for thermal energy storage [16] and through considering a latent thermal energy storage unit to improve the solar utilisation factor of the cycle [17]. The concepts developed in these studies have been expanded into a fully developed experimental cycle, funded by Innovate UK, with this cycle being termed the ST-CHP cycle [18]. This experimental cycle was able to generate up to 0.4 kWe of power output from a micro-turbine connected to a solar-dish receiver, a recuperator, and a low-temperature thermal energy storage unit.

The studies above show that there is potential to develop a CSP power plant to provide electricity through utilising solar energy, however, many of these power plants have minimised performance outputs as a result of the added pressure losses associated with the recuperation and solar hybridisation components required to improve the thermal efficiency of the cycle. To address the impact that pressure losses have on the performance results of a Brayton cycle, Van der Merwe et al. [19] introduced alternative Brayton cycle layouts that make use of various parallel-flow configurations (instead of traditional single-shaft or twin-shaft configurations) to lessen the effect of pressure losses on the results of the power turbine. This study uses radial commercial turbochargers to model the cycle microturbine as done in the studies by Le Roux [15], Le Roux & Sciacovelli [16], De Beer et al. [20], and Butt et al. [21].

The use of automotive turbochargers in a Brayton power plant is a feasible concept as shown by the commercialisation of the Visser et al. [22] 3 kW combined heat and power plant. Additionally, this concept is further feasible for CSP applications due to the radial turbocharger structure allowing for sufficient room for the addition of the required components to form a CSP power plant [23]. However, the downside of using a commercial turbocharger as the microturbine for CSP applications is that these turbochargers operate at low pressure ratios which means that pressure losses result in a greater loss of power output due to the subsequent lower pressure ratio through the turbines. This means that a parallel-flow configuration can be more beneficial due to a lower pressure loss influence on the pressure ratio through the power turbine. This does however depend on the chosen parallel-flow configuration [19].

The study by Van der Merwe et al. [19] (considering parallel-flow cycles) consisted of various simple and recuperated cycles using various cycle split-off points. The study defined low-temperature turbine (LTT) cycles with the power turbine split-off point directly after the compressor outlet, and high-temperature turbine (HTT) cycles with the power turbine split-off point directly after the combustor outlet. The recuperated LTT configuration showed the most potential for development. These configurations have been expanded by Cockcroft & Le Roux

[24] into an intermediate-temperature turbine (ITT) configuration wherein the power turbine split-off point is placed directly after the recuperator cold-side outlet (between the LTT and HTT split-off points), with this configuration showing good overall power output and thermal efficiency performance but with the recuperated LTT having the highest overall thermal efficiency at low pressure ratios.

Cockcroft & Le Roux [25] further expanded the simple and recuperated studies to consider a solar heat input with various solar receiver placements in the unrecuperated solar and recuperated solar cycles, namely with placement options prior to the combustion chamber inlet (SR-CC) and prior to the power turbine inlet (SR-PT). The study by Cockcroft & Le Roux [26] further expanded on the various parallel-flow cycle concepts through directly comparing the results of various simple, recuperated, unrecuperated solar, and recuperated solar parallel-flow cycles to their single-shaft counterparts to determine whether a parallel-flow cycle offers feasible improvements over a single-shaft cycle. This was done through considering different main shaft turbochargers and power turbines. It was shown that the better parallel-flow cycle performance is greatly dependent on the selected main shaft turbocharger. Additionally, when recuperation and solar energy are considered for the cycle, a parallel-flow cycle is better for obtaining the maximum thermal efficiency. Here, the recuperated solar LTT cycle (SR-PT) showed the highest overall feasible cycle thermal efficiency of 23.5 % with a power output of 3 kW at a pressure ratio of 1.6. The study also showed that when greater pressure losses are considered, a parallel-flow cycle, particularly with an LTT or ITT split-off point, offers a better performance response and does not experience the great performance decline that is experienced by a single-shaft cycle.

1.1. Novelty and contribution

The current study seeks to expand on the various solar and recuperated solar parallel-flow cycles by Cockcroft & Le Roux [25,26] through utilising both parallel-flow solar receiver placements by the reference studies. The parallel-flow nature of the cycle configurations in this study, along with the consideration of multi-dish and alternative receiver placements allows for the analyses of systems that have not previously been investigated. These multi-dish parallel-flow cycles are compared to multi-dish unrecuperated solar and recuperated solar single-shaft cycles, with two dish-receiver setups placed in succession of one another prior to the combustion chamber inlet to determine the degree of performance improvement (particularly focusing on thermal efficiency) that is obtained for the various possible parallel-flow and single-shaft multi-dish setups. Thus, this study forms its novelty through considering the influence that the use of two solar receivers, with a multi-dish setup, has on the results of the various cycles and determining whether a multi-dish setup is feasible for implementation. To the authors' knowledge, multi-dish systems have not previously been analysed in the small-scale configurations of the current study, with the consideration of the usage of off-the-shelf automotive turbochargers, with comparisons to single-dish and single-shaft cycles. The multi-dish concept allows for additional innovation through distributing the cycle heat to multiple regions via the parallel-flow cycle so that higher power output can be obtained while lessening the fuel required to operate the cycle. Additionally, the parallel-flow concept allows for the distribution of pressure losses to alternative flow streams in the cycle so as to allow for a maximisation of turbine pressure ratios and a reduction of pressure losses occurring at high temperatures.

Note that the current study follows an analytical analysis of various multi-dish cycles to ascertain the feasibility of these cycles on a theoretical basis. This is however not an analysis of an existing real-world system. Thus, an experimental study would need to be implemented in future work to determine the real-world feasibility of the system. In addition to this, a further limitation in the study persists in the fact that it focusses primarily on a small-scale multi-dish system. Thus, system scalability is not addressed in the current study and can be considered in future work.

1.2. Economic and environmental considerations

On an economic basis, the addition of a recuperator or an additional solar dish-receiver setup would result in additional capital expenditure regarding manufacturing the cycle. An analysis regarding this is not done in the current study due to the study focussing mainly on the feasibility of the multi-dish setup. An economic analysis of the system would need to be done to ascertain real-world system feasibility – an analysis regarding the localised cost of energy or a consideration of the cycle payback period would need to be done. This is particularly important because a recuperator can amount to as much as 30 % of the capital costs of the overall power cycle in a non-solar cycle [27]. In addition to this, the costs associated with implementing a solar dish-receiver setup in the cycle are more difficult to quantify without an in-depth analysis, however, these costs are typically substantial. For reference, the study by Zhu et al. [28] indicates that the addition of solar thermal energy to a coal-fired power plant can add an additional 160 % to the initial capital costs associated with the cycle. The additional costs associated with these components in the cycles addressed in the current study can be considered in future studies.

When considering the environmental impact of the multi-dish setup, a higher thermal efficiency (as per the aim of the study) would allow for a lower environmental impact due to a lower fuel requirement with reference to the power output of the cycle. This lower fuel requirement ascertains that there are fewer emissions produced via the combustion process which thus lowers the environmental impact of the cycle. This also conversely impacts the running costs of the cycle via a reduction of the fuel costs associated with operating the cycle. Thus, economic feasibility is partially addressed in this study via a higher thermal efficiency allowing for a lower fuel cost with reference to the power output of the cycle.

2. Methodology

Different multi-dish configurations are solved for in the current study, as will be introduced following this section. These multi-dish configurations are compared to various unrecuperated solar and recuperated solar single-shaft and parallel-flow configurations, as introduced in the studies by Cockcroft & Le Roux [25,26].

To model the various solar cycle configurations, different pressure ratios are considered and solved for via Python coding, as was done in Ref. [26]. For the unrecuperated solar cycles there are no geometry variables that need to be inputted into Python arrays and thus a wide range, with many intermediate pressure ratios are solved for. These pressure ratios consist of pressure ratios and step sizes as shown in Table 1, as per the pressure ratio ranges in Ref. [26]. For the recuperated solar cycles, the recuperator channel height (in millimetres), b, is subjected to array values consisting of *[1.50, 2.25, 3.00, 3.75, 4.50]*, the number of recuperator channels in a single direction, n, is subjected to array values consisting of *[15, 22.5, 30, 37.5, 45]*, and the compressor pressure ratio is subjected to array values consisting of *[1.4, 1.5, 1.6, 1.8, 2.0, 2.25, 2.5]*, as in the studies by Refs. [24,25,26]. Considering these input arrays, the various cycles are solved for in Python as per the solution procedures in Appendix A. The remaining Python procedures are the same as in the study by Ref. [24], for reference.

Table 1
Pressure ratios and step sizes for unrecuperated solar cycles.

Pressure Ratio Set	Minimum Pressure Ratio	Maximum Pressure Ratio	Step Size
Set 1	1.400	2.000	0.050
Set 2	2.125	2.625	0.125
Set 3	2.750	3.000	0.250

2.1. Cycle layouts

The various unrecuperated solar and recuperated solar configurations are defined in the sections to follow. These layouts directly expand from the layouts defined by Cockcroft & Le Roux [25,26], with the reference parallel-flow receiver placements, before the combustion chamber (SR-CC) (shown in Fig. 1) and before the power turbine (PT-CC) (shown in Fig. 2), being the same as 'SR 1' and 'SR 2' in the parallel-flow layout figures (Fig. 4 and Fig. 6), respectively. For the single-shaft (SS) layouts, the two multi-dish receivers are placed in succession of one another, which is in essence the same as using a larger solar dish for the heat addition but is kept as two different dish-receiver setups in the current study for fair comparison between the various parallel-flow and single-shaft cycles.

Realistically, the easiest way to accomplish the various multi-dish setups is to use a larger dish that is manufactured to allow for the reflection of solar rays into both solar receivers via angling the dish surface towards two individual focal points instead of just one for the single dish/receiver setups. This cycle structure can be achieved through using multiple individual vacuum-membrane facets, as in the study by Swanepoel et al. [18], with each facet aimed towards its respective solar receiver as illustrated in Fig. 3. Note that more components (such as vacuum-membrane facets), are required in the multi-dish cycle to obtain the bigger solar dish. Therefore, an adequate thermal efficiency performance improvement is required in the multi-dish cycle to warrant the implementation of the additional components when considering the capital and operational expenditure associated with the small-scale solar-dish cycle.

Prior to introducing the various multi-dish layouts, the naming conventions used for the parallel-flow cycle split-off points are defined. The first possible split-off point occurs directly after the compressor outlet and thus has the lowest split-off point temperature. This split-off point is termed the low-temperature turbine (LTT) split-off point. The split-off point directly after the cold-side recuperator outlet is termed the intermediate-temperature turbine (ITT) split-off point as a result of having a higher split-off point temperature than the LTT split-off point. A split-off point placement after the combustion chamber outlet is termed the high-temperature turbine (HTT) split-off point. When there is a solar receiver prior to the combustion chamber inlet, the split-off point is termed the solarised intermediate-temperature turbine cycle (ITT(S)) cycle due to having a higher split-off point temperature than the ITT cycle, but not as high of a split-off point temperature as in the HTT split-off point.

Lastly, note that for single-shaft configurations (to be further discussed in the sub-sections to follow), the multi-receiver cycle structure contains two solar-receivers in series. This is essentially equivalent to having a larger solar dish with a larger solar receiver.

2.1.1. Unrecuperated solar cycle layouts

There are four different multi-dish unrecuperated solar cycle configurations in this study, with three of these configurations being parallel-flow configurations, and one being a single-shaft configuration. The three possible multi-dish parallel-flow configurations are shown in Fig. 4 and consist of a multi-dish LTT cycle, a multi-dish ITT(S) cycle, and a multi-dish HTT cycle. These cycles all have different parallel-flow split-off points, with the first solar receiver placed directly before the combustion chamber, and with the second solar receiver placed between each respective split-off point and the power turbine. The unrecuperated solar multi-dish single-shaft configuration is illustrated in Fig. 5 and includes the two solar receivers placed directly in succession between the compressor outlet and the combustion chamber inlet.

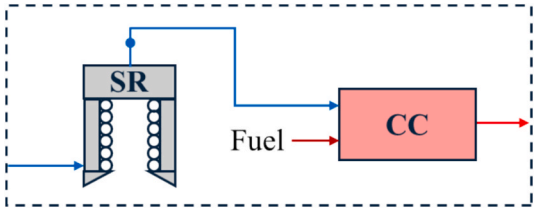

Fig. 1. Solar receiver placement 1 – before the combustion chamber (SR-CC).

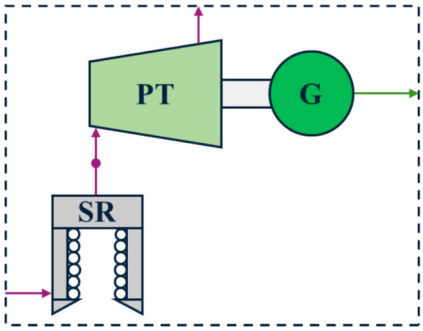

Fig. 2. Solar receiver placement 2 – before the power turbine (SR-PT).

2.1.2. Recuperated solar cycle layouts

For the recuperated solar cycles, there are five possible multi-dish configurations. The first four multi-dish configurations consist of the parallel-flow configurations in Fig. 6. These parallel-flow configurations are the multi-dish LTT configuration, the multi-dish ITT configuration, the multi-dish ITT(S) configuration, and the multi-dish HTT configuration. These parallel-flow configurations utilise a solar receiver placed directly before the combustion chamber, as the first solar receiver, and a solar receiver placed directly before the power turbine, as the second solar receiver. The split-off point position changes to form each parallel-flow configuration type. The solar recuperated multi-dish single-shaft configuration is illustrated in Fig. 7 with two receivers used in succession to form the multi-dish setup, and without the inclusion of the power turbine.

2.2. Component analysis

The cycles are to be analysed using steady-state analysis procedures. The component analysis follows the same structure and analysis as in the studies by Refs. [29] and [24–26], with a simple parallel-flow cycle being verified in the study by Ref. [29]. The component analysis and procedures are therefore not fully detailed in the current study, but a brief overview is provided. In addition to this, sample solution flow charts are provided in Appendix A with the purpose of detailing the solution procedures applied to the various multi-dish setups discussed in Section 2.1. The various Brayton cycles all operate with an intake of ambient air in Pretoria South Africa, at a pressure of 86.6 kPa and at a temperature of 300 K [29]. The cycles also exhaust to the ambient pressure of 86.6 kPa.

Power output and thermal efficiency form primary performance parameters for the various cycles. For the various parallel-flow configurations, the power output depends on the gasifier and power turbine power generation rates, as well as on the required compressor power, however, the gasifier turbine and compressor work rates balance so as to allow the power turbine to be the turbine responsible for the net power output, as in Eq. (1). Note that for the parallel-flow cycles, only the power turbine is coupled to a generator as the gasifier turbine power is used to operate the compressor via their connected shaft. The various single-shaft cycles do not have separate power turbines and thus the net power output is determined using Eq. (2). The subsequent thermal efficiency of each cycle is based on the ratio between the net power output and the heat added to the cycle in the combustion process as detailed by Eq. (3). Note that the thermal efficiency in Eq. (3) is actually the fuel-based thermal efficiency defined by Ref. [25] instead of the total

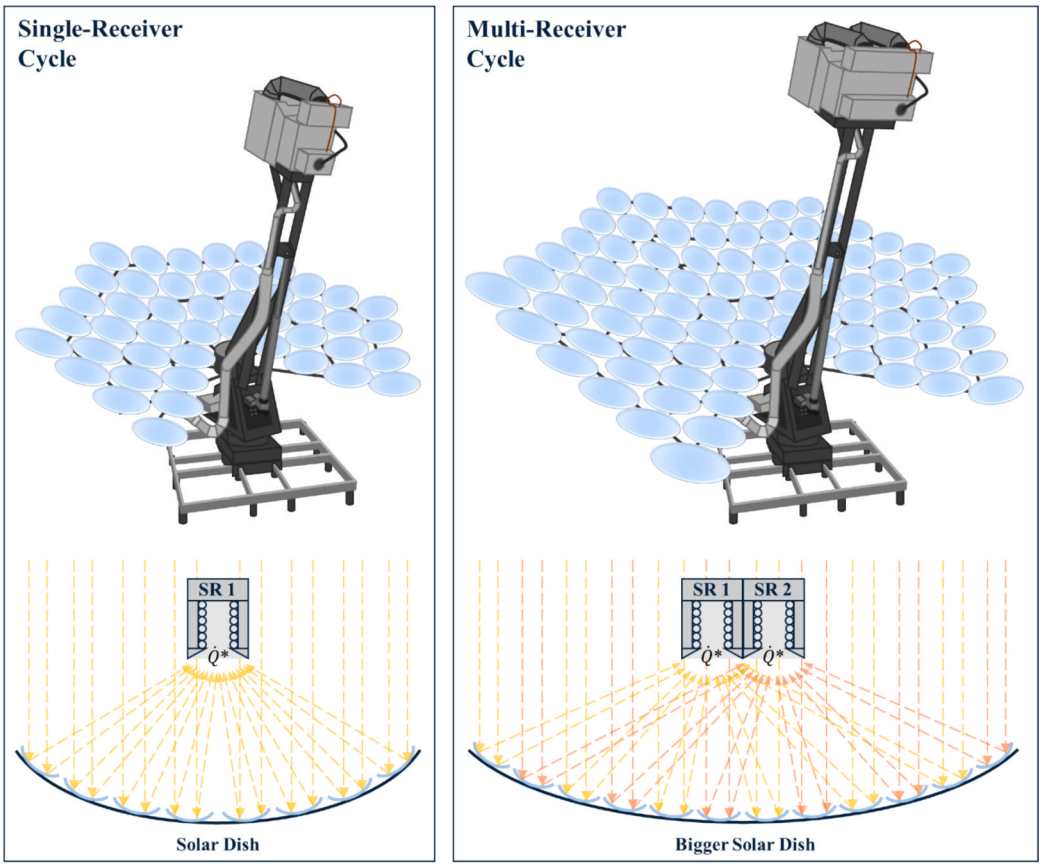

Fig. 3. Single-receiver and multi-receiver cycle structures.

thermal efficiency which would include the addition of solar heat in the denominator of Eq. (3). The reason for defining and using the fuel-based thermal efficiency, rather than the actual thermal efficiency, is to better indicate the obtained power output with reference to the fuel that is added for the operation of the cycle. For simplicity, the fuel-based thermal efficiency is defined simply as thermal efficiency for the remainder of the current study.

$$\dot{W}_{net} = \dot{W}_{gt} + \dot{W}_{pt} - \dot{W}_{comp} = \dot{W}_{pt} \quad (1)$$

$$\dot{W}_{net} = \dot{W}_{gt} - \dot{W}_{comp} \quad (2)$$

$$\eta_{th} = \frac{\dot{W}_{net}}{\dot{Q}_{CC}} \quad (3)$$

Lastly, the current study utilises the off-design application of commercial turbochargers, via the use of turbochargers as microturbines in the cycles. Thus, the resulting turbomachinery operating points occur in regions of the turbocharger flow maps that are off-design with reference to the intended turbocharger operating points. Therefore, the influence of off-design application is accounted for by utilising the compressor and turbine maps when analysing the efficiency of the turbomachinery.

2.2.1. Compressor and turbines

The compressors and turbines in the various cycles are to be solved as adiabatic and non-isentropic turbomachinery components. Commercial turbocharger maps are digitised, using *Webplotdigitizer* [30], to represent the turbomachinery in the various cycles. The data from the digitised turbomachinery maps is extracted and used in the solution algorithms based on a contour mapping approach in Python as detailed by Refs. [24,29]. The coupled gasifier turbine and compressor are represented using the *Garret Motion* [31] G25-550 (AR = 0.92) main shaft turbocharger, in both the parallel-flow and single-shaft cycle configurations. This main shaft turbocharger was selected, from a wide range of turbocharger options, based on its good compatibility results and high thermal efficiency as shown in the study by Cockcroft & Le Roux [26]. For the power turbine, the GBC14-200 and the GBC17-250 were identified as good power turbine options and thus the results of the various parallel-flow configurations with these power turbine options were considered in the current study.

Seeing as commercial *Garrett Motion* turbochargers are used in the current study, the maximum allowable turbine inlet temperature of 950 °C, as specified by the turbocharger manufacturer, must be adhered to [32]. As a conservative consideration of this temperature limit, the current study considered the maximum allowable turbine inlet temperature as 1200 K (927 °C). This conservative temperature limit has also been considered in the study by Ref. [16].

2.2.2. Combustion chamber

LPG (consisting of 60 % propane and 40 % butane [33]) is combusted with the air that enters the combustion chamber. This is done to supply the required heat to the cycle that is not provided by the recuperator and/or solar receiver under the consideration that 6 % of the incoming combustion chamber pressure is lost in the combustion process as determined for annular combustion chambers in the study by Lefebvre & Ballal [34]. The chemical reaction equation for this process is considered, along with the molar product and reactant relations, to solve for this process via an interpolation process and relations for the air–fuel ratio, shown in Eq. (4), and via the determination of the adiabatic flame temperature for the reaction. This adiabatic flame temperature is solved for in a parallel-flow cycle based on the consideration that there is a specific mass flow rate and inlet temperature (for each cycle design point) to the gasifier turbine to ascertain that the gasifier turbine produces the required amount of power to operate the compressor without

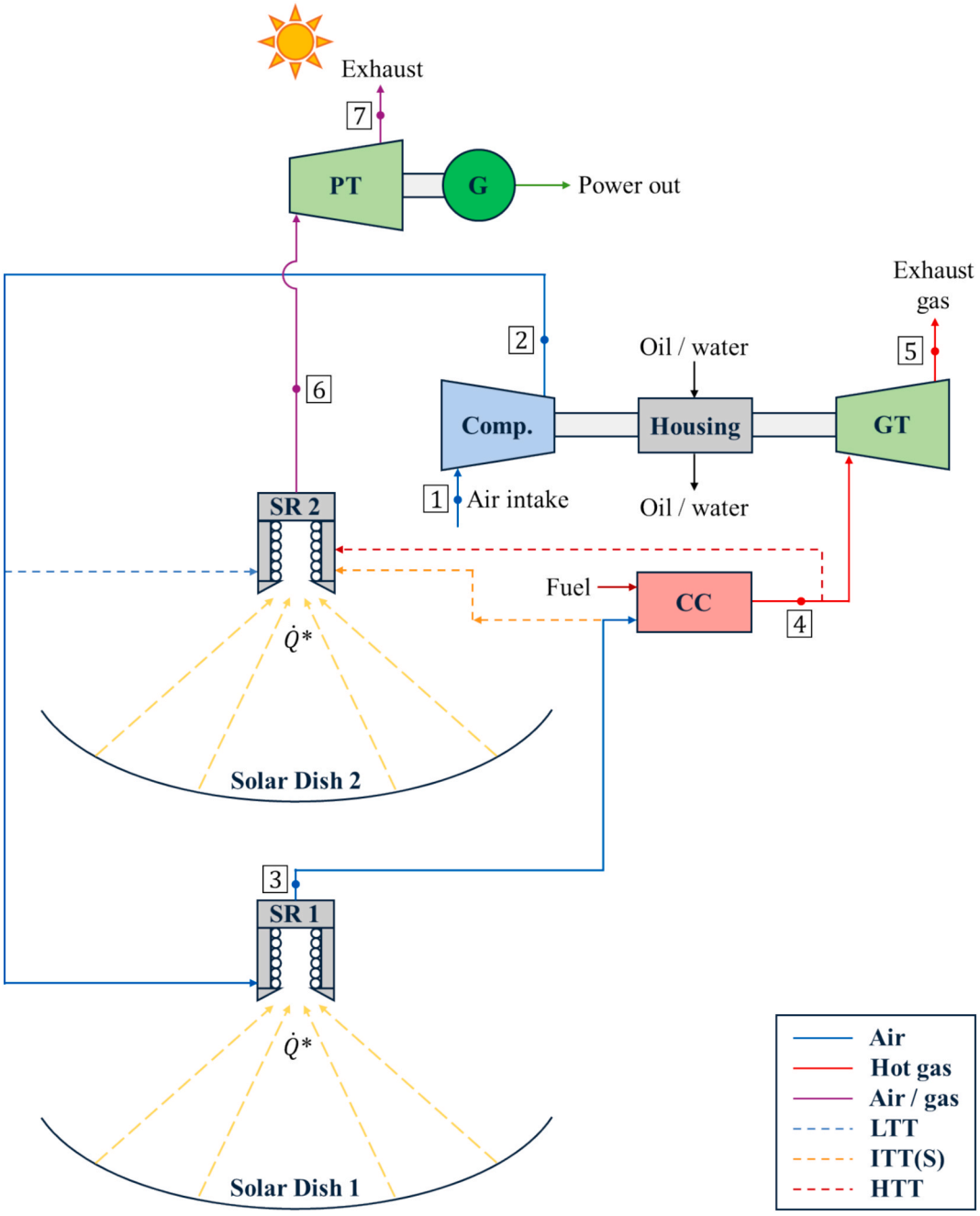

Fig. 4. Unrecuperated solar parallel-flow multi-dish configuration options.

requiring any additional cycle power inputs in a steady-state analysis. This is further detailed by Cockcroft & Le Roux [29]. When it comes to a single-shaft cycle configuration, considering that the gasifier turbine inlet temperature may not be greater than 1200 K, the adiabatic flame temperature is assumed to equate to this temperature limit. Note that in the various single-shaft and parallel-flow cycles, no heat loss to the environment is considered in the combustion process.

$$AFR_{mass} = AFR_{mole}\frac{M_{air}}{M_{LPG}} = \frac{\dot{n}_{air}}{\dot{n}_{LPG}}\frac{M_{air}}{M_{LPG}} \quad (4)$$

2.2.3. Recuperator

Nellis & Pfotenhauer [35] defined a formulation for solving for a flat-plate heat exchanger model, considering various heat losses, using the effectiveness-NTU method. This formulation has been utilised by Le Roux & Sciacovelli [16] to model the flat-plate recuperator, defined in terms of geometry variables, used in the reference Brayton cycle. Further assumptions regarding the recuperator are as in the reference study by Le Roux & Sciacovelli [16]. The recuperator consists of a channel width, a, a channel height, b, a recuperator length, L_{rec}, a plate thickness, t, and the number of channels in a single-direction, n. Only b and n are varied in the current study, with a, t, and L_{rec} being kept constant at 0.225 m, 0.5 mm, and 1.5 m, respectively, as in the study by Ref. [24]. Note that, as in Refs. [24,26], the best-case recuperator geometry for each recuperated solar cycle configuration (detailed in Section 2.1.2) is selected dependent on the best-case thermal efficiency within the cycle temperature limitations. When the various recuperator geometries do not obtain cycle solutions within the gasifier turbine inlet temperature limitation, the geometry is selected that allows for the lowest gasifier turbine inlet temperature instead of the best-case thermal efficiency. The results with these high temperatures are not feasible for operation

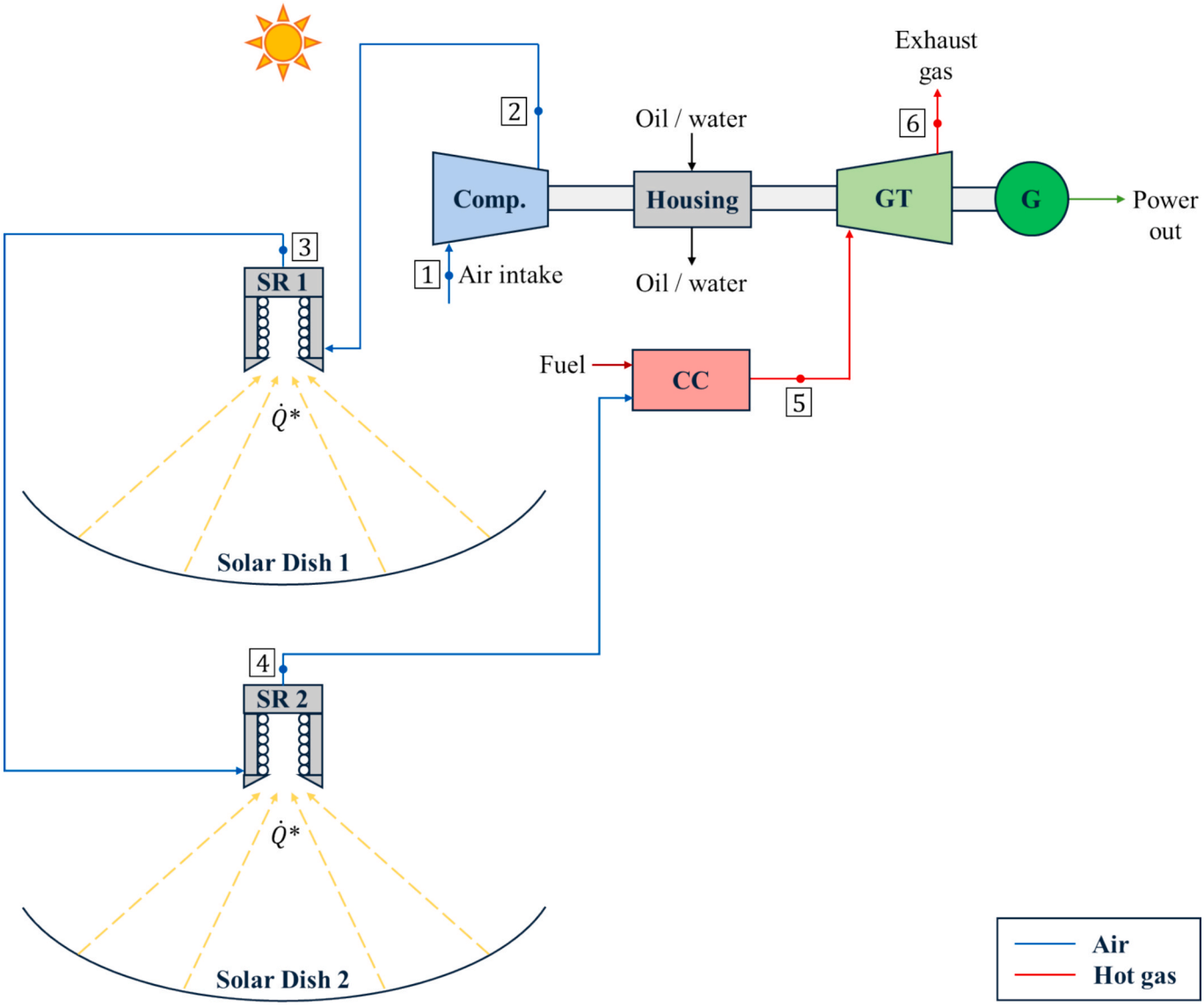

Fig. 5. Unrecuperated solar single-shaft multi-dish configuration.

(due to the high cycle temperatures) but are still presented for comparison purposes.

2.2.4. Solar receiver

The solar receiver model used to represent both solar receivers in the various multi-dish configurations, is based on the rectangular open-cavity tubular receiver model by Le Roux et al. [13] and is further adapted and detailed in the study by Cockcroft & Le Roux [25]. The study by Ref. [25] also includes a verification procedure regarding the solar receiver model, with the same solar receiver model setup being used in both the current study and in Ref. [25]. These models make use of a solar dish with an approximate dish area of 18 m^2 with a 4.8 m diameter [13]. The solar irradiance is assumed to be 1000 W/m^2 and the dish is further defined to have an optical error of 10 mrad [13]. The solar rays that are reflected from the solar dish are traced via solar flux mapping using a SolTrace model [36]. As a direct result of the design restrictions of the materials used to construct the solar receiver, the receiver tubes' surface temperatures may not exceed 1200 K [13]. The studies by Refs. [13,25] can be further referred to for more details regarding the solar receiver setup and assumptions.

Furthermore, Eq. (5) is used to determine the solar receiver heat transfer rate to the working fluid under the consideration of radiation, conduction, and convection heat losses. A Gaussian elimination scheme is used to solve for the heat transfer rate in Eq. (5) as initially done by Le Roux et al. [13]. The solar receiver efficiency is then determined using the calculated heat transfer rate and the total solar heat via the relation in Eq. (6) [13].

$$\begin{aligned}\dot{Q}_{\mathrm{net,n}} = \; & \dot{Q}_{\mathrm{n}}^{*} - A_{\mathrm{n}}\sum_{\mathrm{j}=1}^{\mathrm{N}} F_{\mathrm{n-j}}\left(\varepsilon_{\mathrm{n}}\sigma T_{\mathrm{s,n}}^{4} - \varepsilon_{\mathrm{j}}\sigma T_{\mathrm{s,j}}^{4}\right) \\ & - A_{\mathrm{n}}F_{\mathrm{n-0}}\left(\varepsilon_{\mathrm{n}}\sigma T_{\mathrm{s,n}}^{4} - \varepsilon_{\mathrm{j}}\sigma T_{0}^{4}\right) - \lambda_{\mathrm{SR,n}}A_{\mathrm{n}}\left(T_{\mathrm{s,n}} - T_{0}\right) \\ & - \frac{A_{\mathrm{n}}\left(T_{\mathrm{s,n}} - T_{0}\right)}{\frac{1}{\lambda_{\mathrm{o}}} + \frac{t_{\mathrm{ins}}}{k_{\mathrm{ins}}}}\end{aligned} \tag{5}$$

$$\eta_{\mathrm{SR}} = \frac{\dot{Q}_{\mathrm{net}}}{\dot{Q}^{*}} \tag{6}$$

3. Results

The results of the various multi-dish unrecuperated solar and recuperated solar cycles are compared to each other and the various single-dish solar cycles by Cockcroft & Le Roux [25,26]. The single-dish cycles

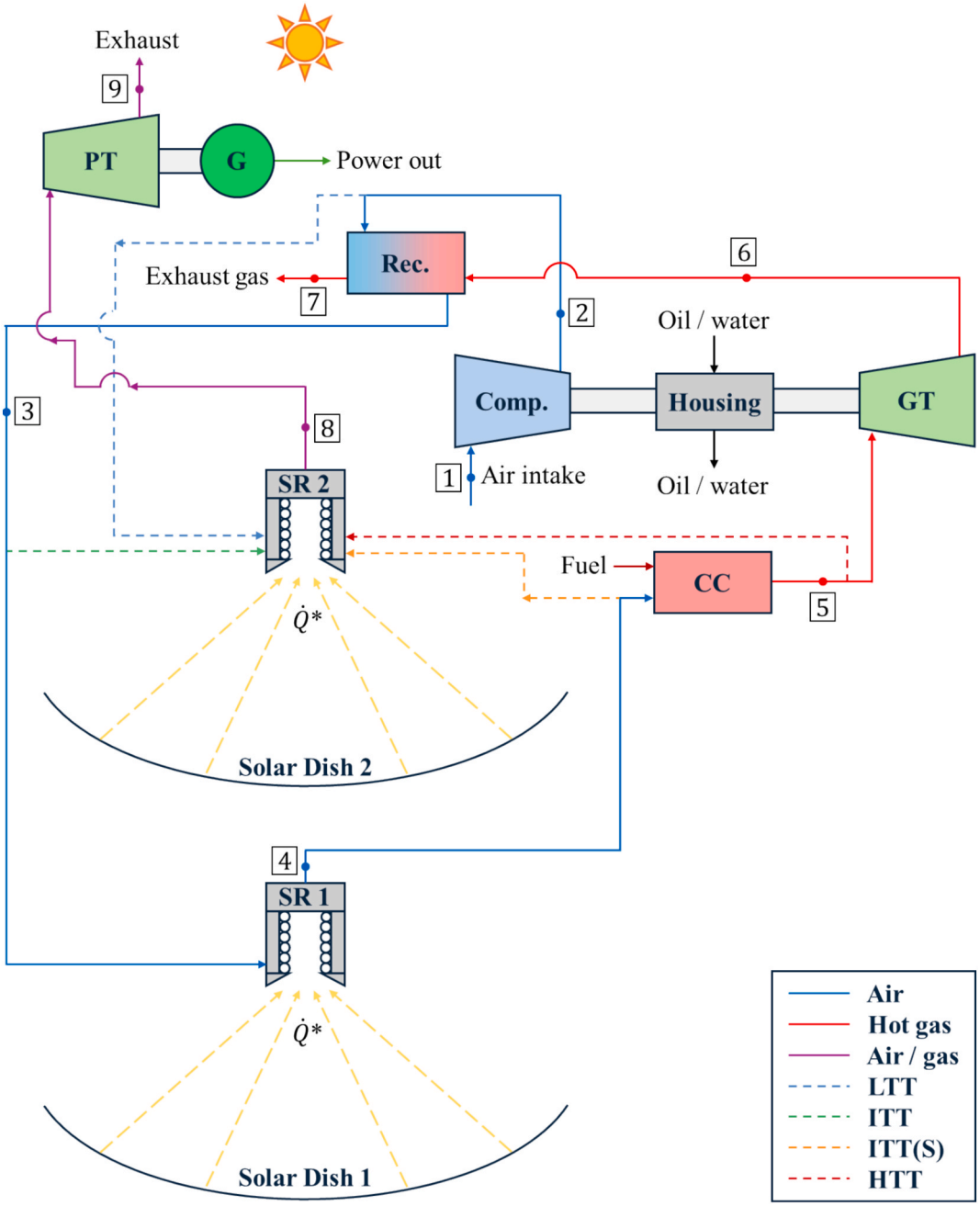

Fig. 6. Recuperated solar parallel-flow multi-dish configuration options.

have been compared to one another in-depth in Refs. [25,26] and thus the primary focus of the results analysis in the current study is to determine the best multi-dish configuration performance.

3.1. *Unrecuperated solar cycle results*

The various unrecuperated solar cycle results are analysed. For this, the power output and thermal efficiency, the cycle temperatures that are limited to 1200 K, and the solar receiver efficiency are discussed.

3.1.1. *Power output and thermal efficiency*

The power output results of the various single-dish cycles, with different receiver placements, as well as the newly obtained multi-dish power output results, are shown in Fig. 8. Here, it is shown that a multi-dish setup reduces the overall power output of the single-shaft cycle (with the single-shaft cycle obtaining the highest overall power output). Similar power output results are obtained for the multi-dish LTT and ITT(S) cycles in comparison to their respective single-dish cycles with the second receiver placement (SR-PT), when comparing the same pressure ratio.

Furthermore, it is shown in Fig. 8 that the parallel-flow LTT and ITT (S) cycles are compatible to a higher pressure ratio range when the GBC14-200 is used as the power turbine, but greater power outputs are obtained when the GBC17-250 is used as the power turbine, when considering the maximum pressure ratios of operation for each configuration. Note that the HTT split-off point does not obtain any results when the multi-dish or second receiver placement (SR-PT) is used.

When considering the thermal efficiency results of the various cycles, Fig. 9 shows that both the single-dish and multi-dish single-shaft cycles mostly have much higher thermal efficiencies than the parallel-flow cycles. This is in line with the findings by Cockcroft & Le Roux [26], where in a unrecuperated solar cycle with the G25-550 (AR = 0.92) as

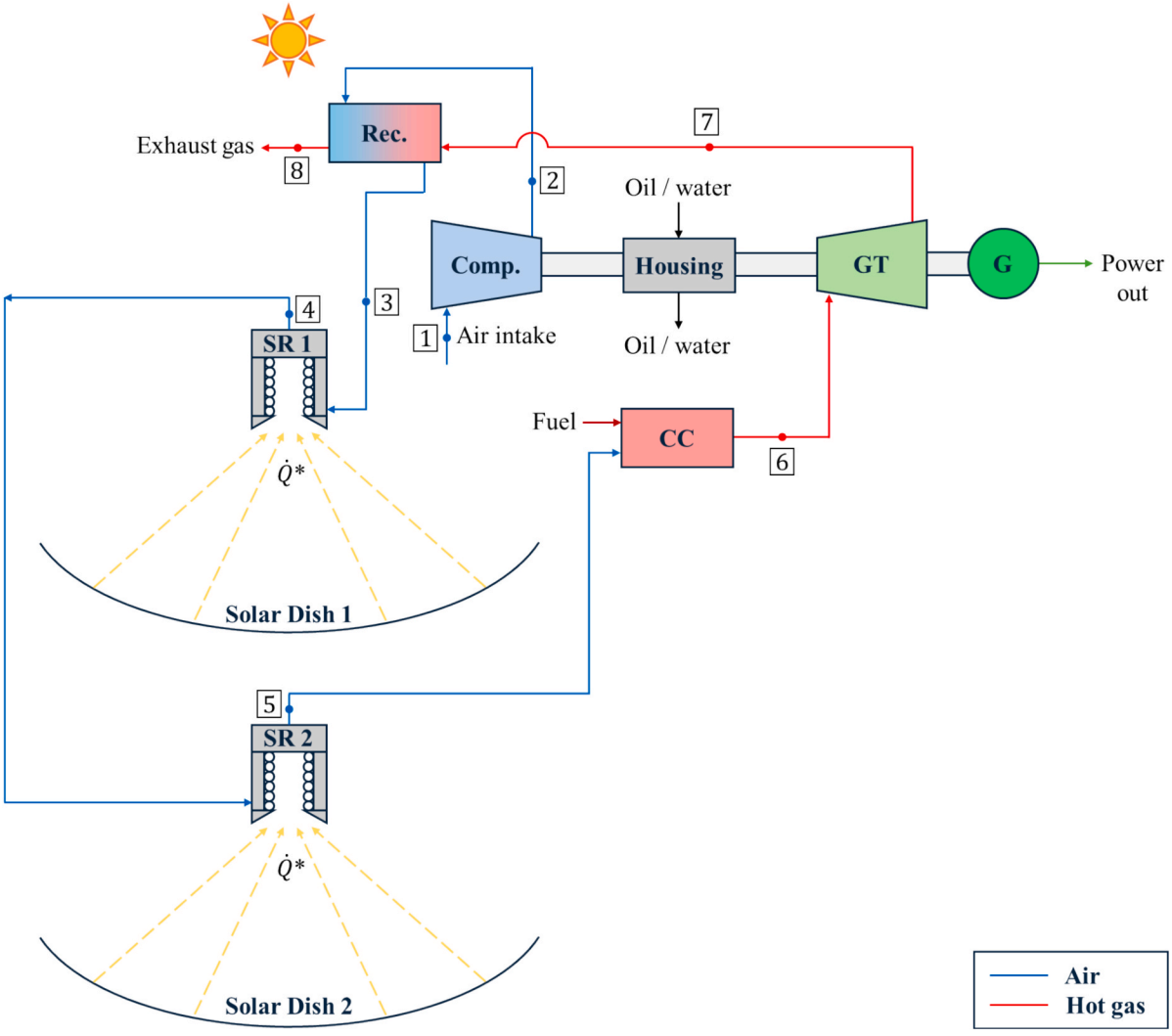

Fig. 7. Recuperated solar single-shaft multi-dish configuration.

the main shaft turbocharger, none of the parallel-flow cycles offer better performance than the single-shaft cycle. Thus, this finding remains the same even for multi-dish cycle setups. For the best cycle performance, it is shown in Fig. 9 that the multi-dish single-shaft cycle offers the best overall thermal efficiency of 11.68 % with a power output of 19.89 kW (Fig. 8) at a compressor pressure ratio of 3.

For the single shaft cycle, which is the best single-dish and multi-dish cycle in terms of obtaining the highest thermal efficiency and power output, a multi-dish cycle adds a percentage improvement in thermal efficiency of between 5.9 % and 12.4 % to the cycle, as per Fig. 9. Fig. 9 also shows that the greatest thermal efficiency improvement occurs at low pressure ratios and decreases to 5.9 % at the highest simulated pressure ratio, considering the same pressure ratio. This comes at a power output reduction of between 3.8 % and 12.5 %. The highest power output reduction occurs at the lowest simulated pressure ratio and the lowest power output reduction occurs at the highest simulated pressure ratio. Thus, for the best performing simple-solar cycle, consisting of the single-shaft cycle, a multi-dish setup may not add a great enough improvement to the cycle performance to warrant the additional capital costs associated with a multi-dish set-up. This is due to the added pressure drop and heat loss through the use of the additional receiver.

3.1.2. Temperatures

When analysing the temperature limits of the cycles, the multi-dish LTT and ITT(S) cycles with the GBC17-250 as the power turbine have high gasifier turbine inlet temperatures (that exceed the limit of 1200 K) at high pressure ratios where these cycles offer the best performance, as shown in Fig. 10. For this same power turbine, both the LTT (SR-CC) and ITT(S) cycles exceed the maximum allowable gasifier turbine inlet temperature for each simulated pressure ratio. The gasifier turbine inlet temperatures are within the allowable limit for all the parallel-flow cycles when the GBC14-200 is used as the power turbine, with the exception of the LTT (SR-CC) cycle at pressure ratios less than 1.45. None of the parallel-flow cycles have power turbine inlet temperatures that exceed the limit of 1200 K, as per Fig. 11. The multi-dish ITT(S) cycle with the GBC14-200 as the power turbine has solar receiver surface temperatures for the second solar receiver that exceed the limit of 1200 K at pressure ratios less than 1.5, as shown in Fig. 12, and is not supported for operation at low pressure ratios. The remaining cycle receiver surface temperatures are within the allowable limit.

3.1.3. Solar receiver efficiency

When analysing the solar receiver efficiencies, via Fig. 13, it is shown that for each multi-dish configuration, the second receiver has the lowest receiver efficiency, with the multi-dish ITT(S) cycle showing the lowest overall solar receiver efficiency for the second receiver. This multi-dish ITT(S) cycle shows the highest solar receiver efficiencies for the first receiver in a multi-dish cycle. The multi-dish LTT cycle with the GBC17-250 as the power turbine is shown to have the highest solar receiver efficiencies when considering the second solar receiver. The

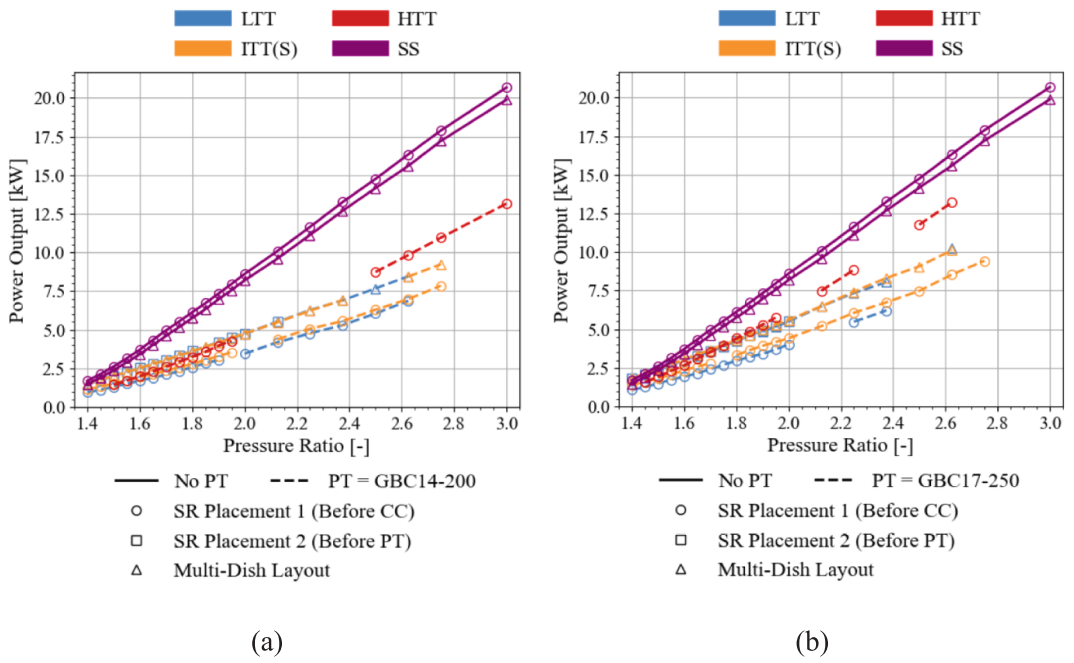

Fig. 8. Power output as a function of pressure ratio for various parallel-flow and single-shaft single-dish and multi-dish unrecuperated solar cycle configurations with (a) the GBC14-200 as the PT and (b) the GBC17-250 as the PT. Note that the single-dish results were reproduced from Refs. [25,26] for comparison purposes.

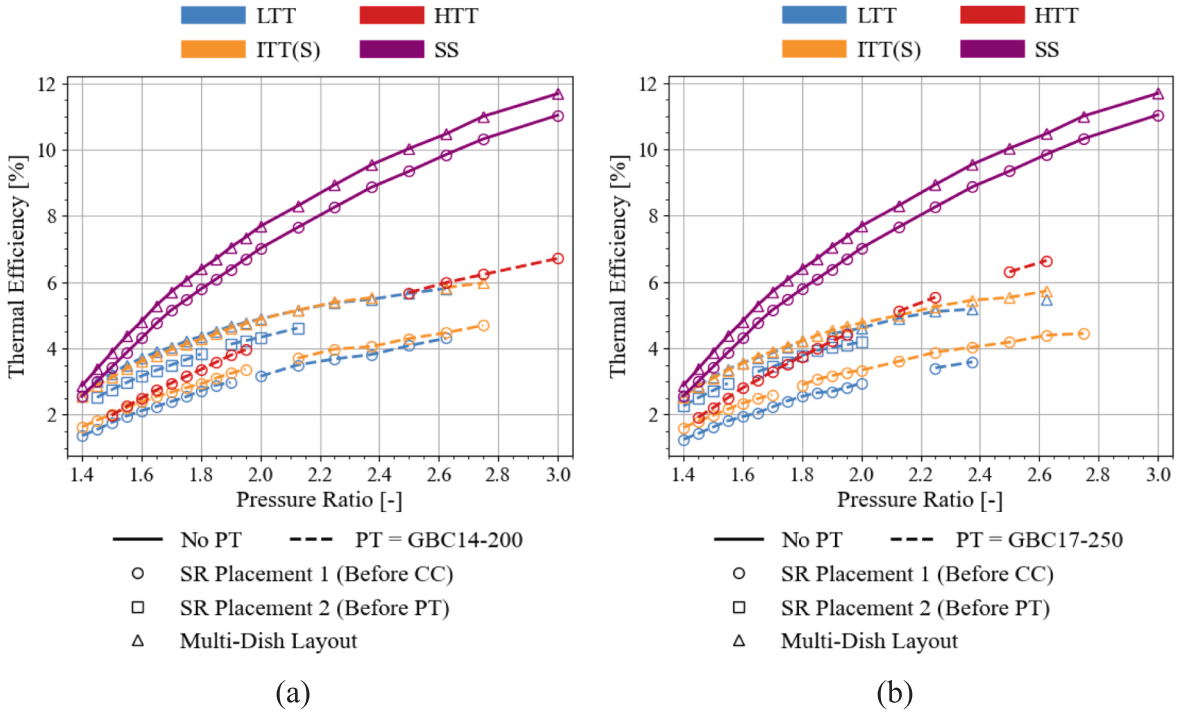

Fig. 9. Thermal efficiency as a function of pressure ratio for various parallel-flow and single-shaft single-dish and multi-dish unrecuperated solar cycle configurations with (a) the GBC14-200 as the PT and (b) the GBC17-250 as the PT. Note that the single-dish results were reproduced from Refs. [25,26] for comparison purposes.

solar receiver efficiency for the first receiver is negligibly different when comparing the results of the single-shaft and multi-dish single-shaft cycles. This is due to the placement of the first multi-dish receiver in the multi-dish single-shaft cycle not deviating in comparison to the single-dish single-shaft cycle, due to both cycles having the first receiver directly after the compressor outlet. The single-shaft and multi-dish single-shaft cycles have the lowest receiver efficiencies for the first receiver placement.

3.2. *Recuperated solar cycle results*

The various recuperated solar cycle results are analysed. For this, the power output and thermal efficiency, the cycle temperatures that are limited to 1200 K, and the solar receiver efficiency and recuperator effectiveness values are discussed. The optimised geometry values used to generate the recuperated cycle results are detailed in Appendix B.

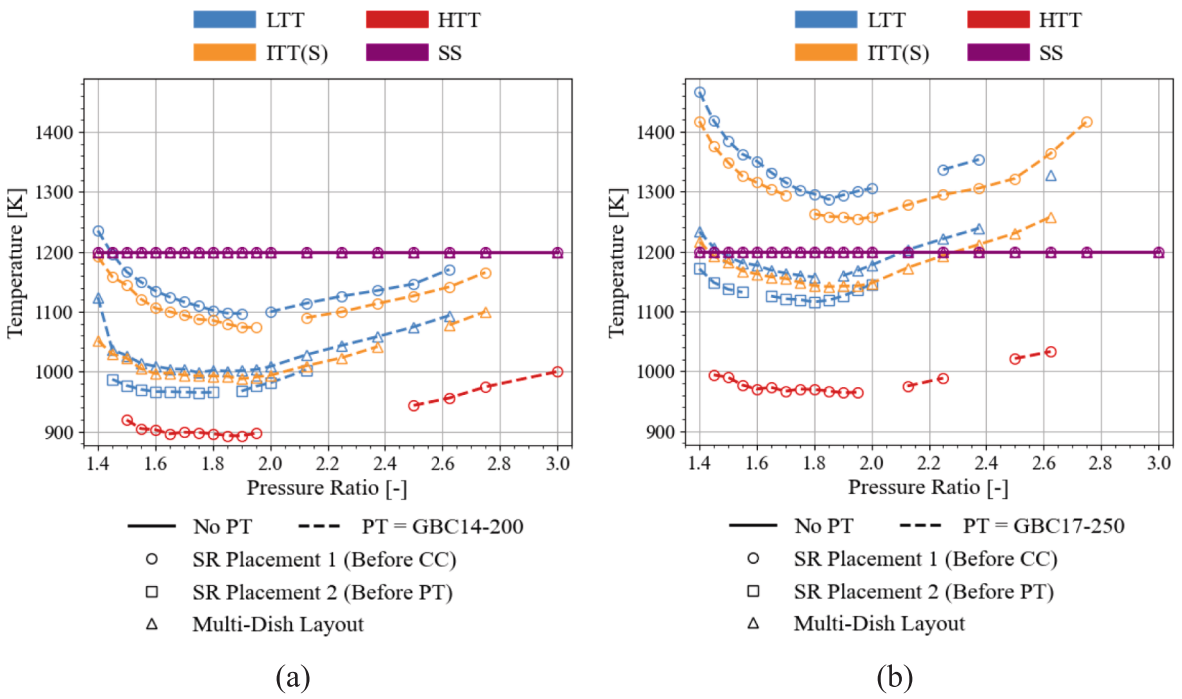

Fig. 10. GT inlet temperature as a function of pressure ratio for various parallel-flow and single-shaft single-dish and multi-dish unrecuperated solar cycle configurations with (a) the GBC14-200 as the PT and (b) the GBC17-250 as the PT. Note that the single-dish results were reproduced from Refs. [25,26] for comparison purposes.

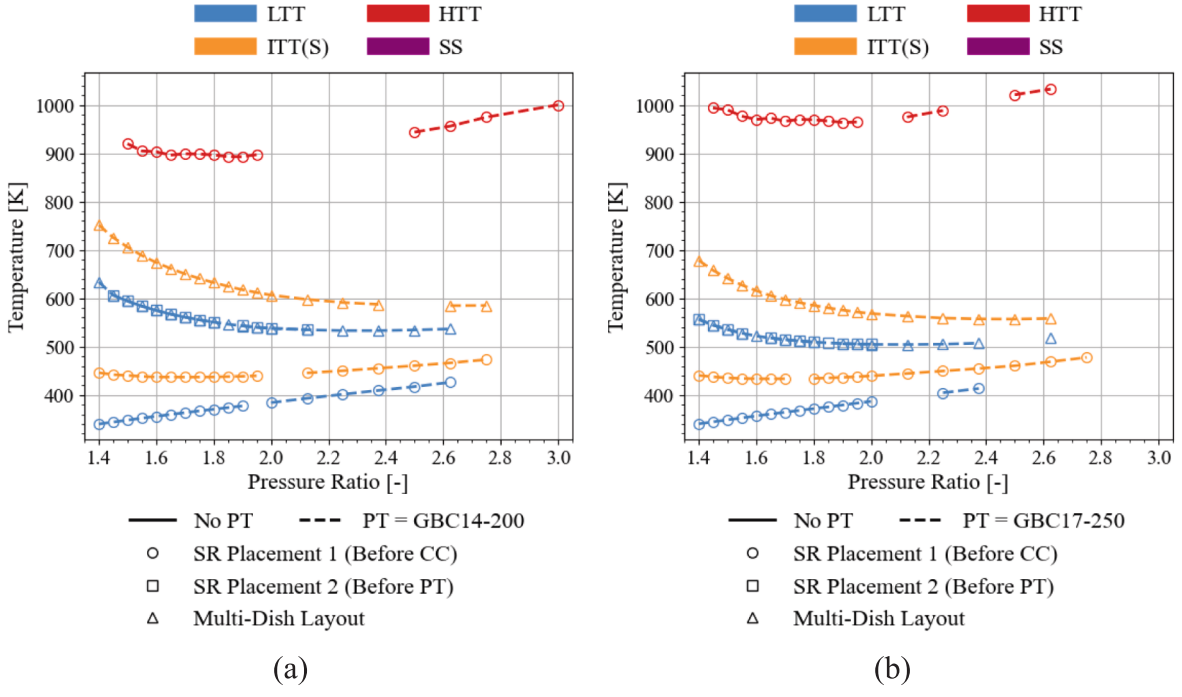

Fig. 11. PT inlet temperature as a function of pressure ratio for various parallel-flow and single-shaft single-dish and multi-dish unrecuperated solar cycle configurations with (a) the GBC14-200 as the PT and (b) the GBC17-250 as the PT. Note that the single-dish results were reproduced from Refs. [25,26] for comparison purposes.

3.2.1. Power output and thermal efficiency

For the various recuperated solar cycles, the power output results are shown in Fig. 14. This figure shows that when comparing the power output of single-dish and multi-dish single-shaft cycles, the multi-dish cycle produces between 0.41 kW (at a pressure ratio of 1.4) and 1.59 kW (at a pressure ratio of 2.5) less power than the single-dish cycle, depending on the pressure ratio. For the LTT parallel-flow cycles, the multi-dish cycles produce negligibly different power output results to their single-dish counterparts with the second receiver placement, which means that in an LTT parallel-flow cycle, there is no loss in power output when utilising a multi-dish setup. There is a slightly more visible loss in power output in the ITT and ITT(S) multi-dish parallel-flow

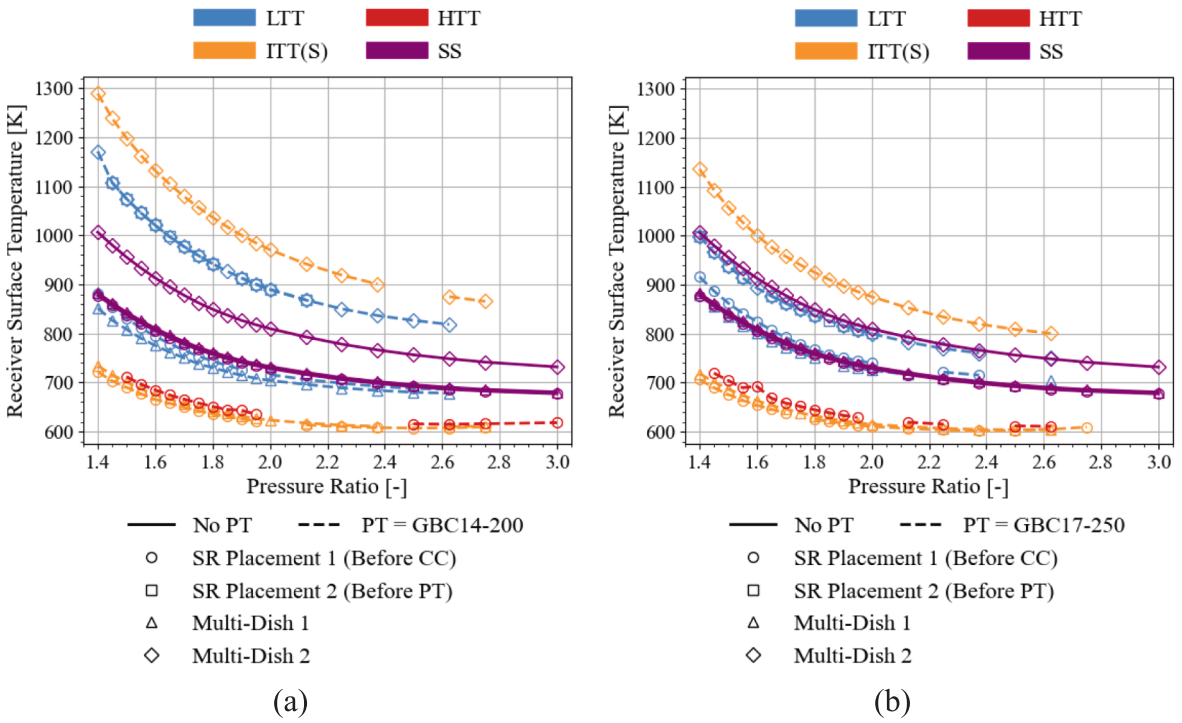

Fig. 12. Maximum solar receiver surface temperature as a function of pressure ratio for various parallel-flow and single-shaft single-dish and multi-dish unrecuperated solar cycle configurations with (a) the GBC14-200 as the PT and (b) the GBC17-250 as the PT. Note that the single-dish results were reproduced from Refs. [25,26] for comparison purposes.

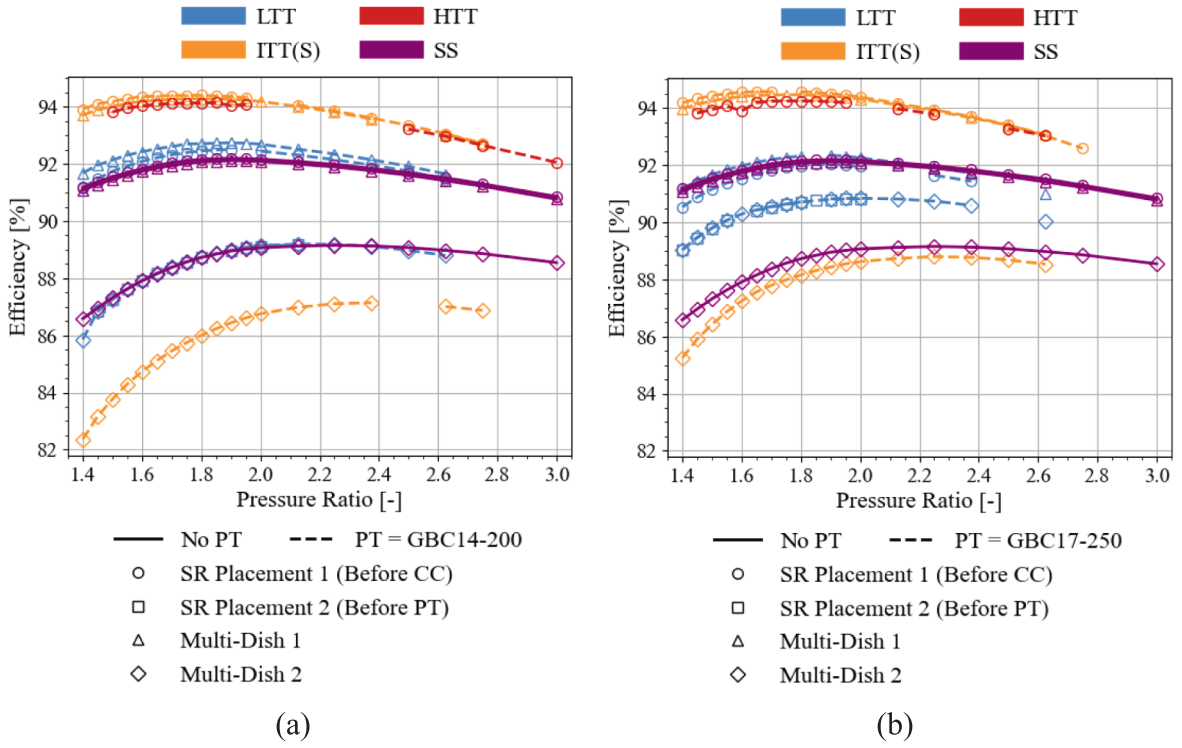

Fig. 13. Solar receiver efficiency as a function of pressure ratio for various parallel-flow and single-shaft single-dish and multi-dish unrecuperated solar cycle configurations with (a) the GBC14-200 as the PT and (b) the GBC17-250 as the PT. Note that the single-dish results were reproduced from Refs. [25,26] for comparison purposes.

cycles, with reference to their respective single-dish counterparts with the second receiver placement. For the HTT cycles, the multi-dish cycle produces similar power outputs to the HTT cycle with the first receiver placement.

Prior to discussing the thermal efficiency results of the single-dish and multi-dish single shaft cycles and the multi-dish LTT cycle with

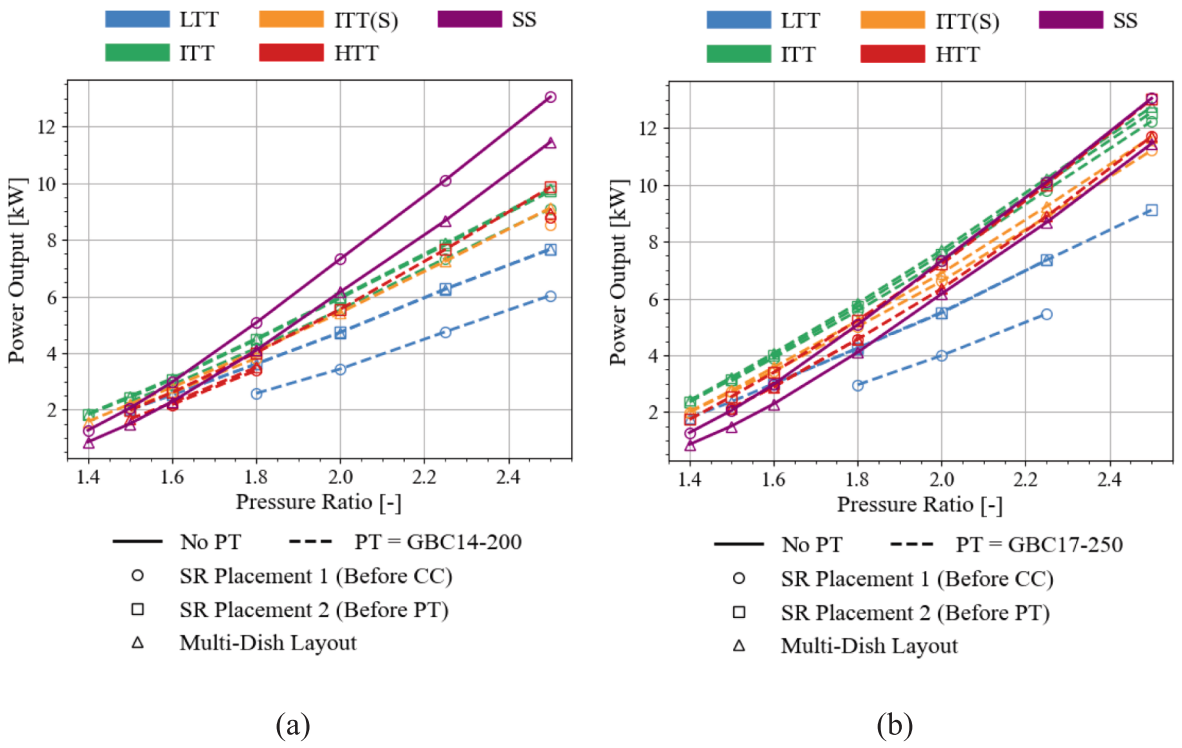

Fig. 14. Power output as a function of pressure ratio for various parallel-flow and single-shaft single-dish and multi-dish recuperated solar cycle configurations with (a) the GBC14-200 as the PT and (b) the GBC17-250 as the PT. Note that the single-dish results were reproduced from Refs. [25,26] for comparison purposes.

the GBC14-200 power turbine, note that these cycles are not supported for operation at pressure ratios less than 1.75 for the single-dish single-shaft cycle, 1.81 for the multi-dish single-shaft cycle, and 1.6 for the multi-dish LTT cycle with the GBC14-200 power turbine. This is as a result of high solar receiver surface temperatures, as will be shown in Fig. 18. Note that much higher thermal efficiency values can be obtained for these cycles at lower pressure ratios, but the maximum solar receiver surface temperatures are too high for these cycles at these lower pressure ratios. Therefore, higher thermal efficiency occurs under conditions that are not feasible for cycle operation. The higher thermal efficiency values are also not shown in the scale of the plot in Fig. 15 to better illustrate the feasible results of the various cycles. The remaining gasifier turbine

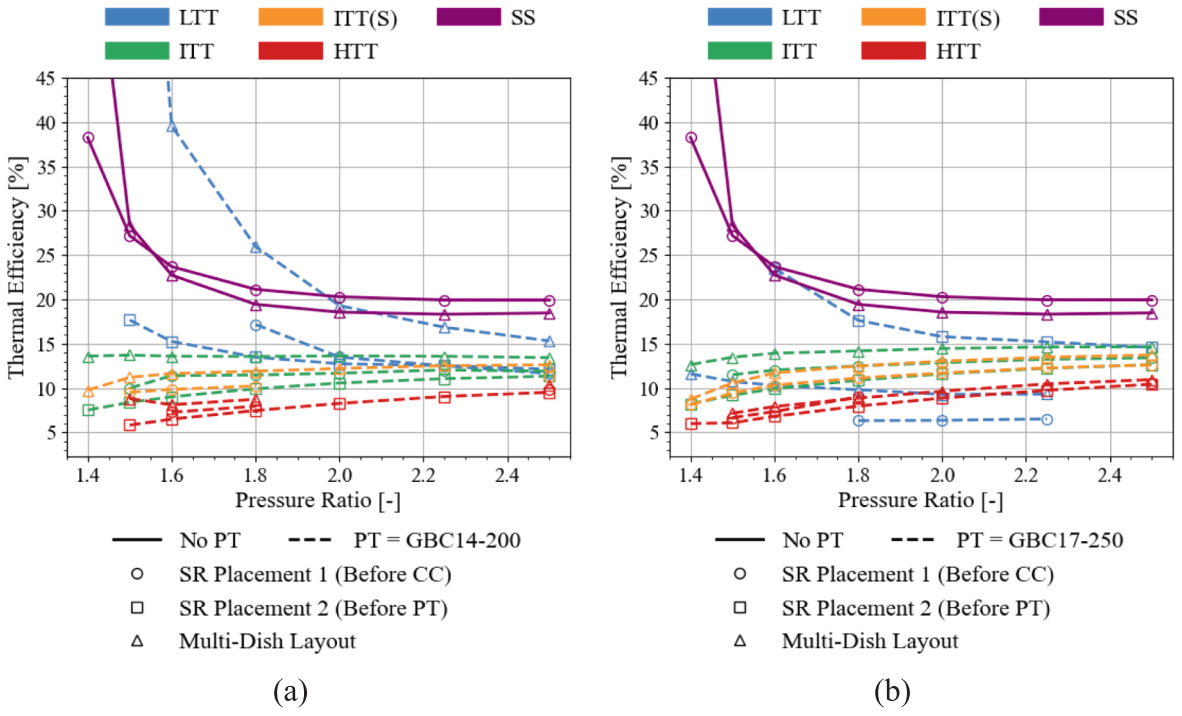

Fig. 15. Thermal efficiency as a function of pressure ratio for various parallel-flow and single-shaft single-dish and multi-dish recuperated solar cycle configurations with (a) the GBC14-200 as the PT and (b) the GBC17-250 as the PT. Note that the single-dish results were reproduced from Refs. [25,26] for comparison purposes.

and power turbine inlet temperatures are all within range for this multi-dish LTT cycle with the GBC14-200 power turbine (as will be shown in Fig. 16 and Fig. 17).

When analysing the thermal efficiency of the various cycles, under the consideration of the maximum allowable solar receiver surface temperatures, Fig. 15 shows that the highest overall thermal efficiency is obtained for the multi-dish LTT cycle with the GBC14-200 as the power turbine. This high thermal efficiency amounts to 39.6 % at a pressure ratio of 1.6, with a power output of 2.5 kW (as per Fig. 14). Via Fig. 15, this high thermal efficiency far outperforms the highest feasible multi-dish single-shaft cycle thermal efficiency of 21.1 % (with a power output of 4.6 kW), as well as the highest feasible single-dish single-shaft cycle thermal efficiency of 21.8 % (with a power output of 4.2 kW) – due to the inability of these cycles to operate at lower pressure ratios while remaining within all the temperature constraints applied to the cycles. This means that the maximum feasible thermal efficiency of the multi-dish single-shaft cycle is 3.2 % lower than that of the single-dish single-shaft cycle. Due to high gasifier turbine inlet temperatures (of greater than 1200 K), a poorer performing recuperator geometry is selected for the multi-dish LTT cycle when the GBC17-250 is used as the power turbine (see Appendix B for reference). This is why the multi-dish LTT with the GBC17-250 as the power turbine does not offer higher thermal efficiency results.

Fig. 15 also shows that the multi-dish single-shaft cycle offers much better thermal efficiency results than the single-dish single-shaft cycle at low pressure ratios. The LTT (SR-PT) cycle with the GBC17-250 as the power turbine produces a power output of 3 kW with a thermal efficiency of 23.5 % at a pressure ratio of 1.6 and thus achieves better feasible maximum thermal efficiency results than both the single-dish and the multi-dish single-shaft cycles. This means that when it comes to obtaining the overall highest thermal efficiency results, the multi-dish LTT with the GBC14-200 as the power turbine is the best option for further investigation and the LTT (SR-PT) cycle with the GBC17-250 as the power turbine is the second-best option for further investigation, with both of these cycles offering better thermal efficiency values than both the single-shaft and multi-dish single-shaft cycles. The multi-dish LTT cycle with the GBC14-200 as the power turbine has a 68.5 % greater maximum thermal efficiency than the LTT (SR-PT) cycle with the GBC17-250 as the power turbine, an 81.7 % greater maximum thermal efficiency than the single-dish single-shaft cycle, and an 87.7 % greater maximum thermal efficiency than the multi-dish single-shaft cycle.

3.2.2. Temperatures

With regard to gasifier turbine inlet temperatures, Fig. 16(a) shows that none of the parallel-flow cycles with the GBC14-200 as the power turbine exceed the maximum allowable gasifier turbine inlet temperature of 1200 K, except for the slightly too high gasifier turbine inlet temperatures of the LTT (SR-CC) cycle at pressure ratios exceeding 2.4. However, when the GBC17-250 is used as the power turbine, Fig. 16(b) shows that the gasifier turbine inlet temperatures are too high for the LTT (SR-CC) cycle and the multi-dish LTT cycle for the entire simulated pressure ratio range.

Furthermore, Fig. 16(b) shows that the ITT(S) (SR-CC) cycle with the GBC17-250 as the power turbine has gasifier turbine inlet temperatures that exceed the limit of 1200 K at pressure ratios less than 1.54. Additionally, the multi-dish ITT(S) cycle with the GBC17-250 as the power turbine has gasifier turbine inlet temperatures that exceed the specified limit at pressure ratios less than 1.46. The LTT (SR-PT) cycle with the GBC17-250 power turbine also has gasifier turbine inlet temperatures, beyond the limit of 1200 K, at pressure ratios greater than 1.95. The power turbine inlet temperatures are within the limit of 1200 K for every simulated parallel-flow cycle for both power turbine options, as shown in Fig. 17.

Fig. 18 shows that all the multi-dish cycles have solar receiver surface temperatures that exceed the limit of 1200 K at low pressure ratios. This is particularly an issue for the second receiver placement in the multi-dish parallel-flow and single-shaft cycles, with the exclusion of the multi-dish LTT cycles due to the low-temperature setup and the subsequent low solar receiver surface temperatures of its second solar receiver. These high solar receiver surface temperatures, while considering both solar receivers with the GBC14-200 as the parallel-flow power turbine, result in the multi-dish LTT cycle only being operable at pressure ratios greater than 1.6, the multi-dish ITT cycle only being operable at pressure ratios greater than 1.73, the multi-dish ITT(S) cycle only being operable at pressure ratios greater than 1.94, the multi-dish single-shaft cycle only being operable at pressure ratios greater than 1.81, and the multi-dish HTT cycle not being operable at all due to high receiver surface temperatures. This is under the assumption that there is a 1200 K material limit for the solar receiver. This temperature limit depends on the material choice and can therefore be increased, typically at an additional cost.

When the GBC17-250 is used as the power turbine, as a result of high solar receiver surface temperatures, the multi-dish LTT cycle is only operable at pressure ratios greater than 1.64, the multi-dish ITT cycle is

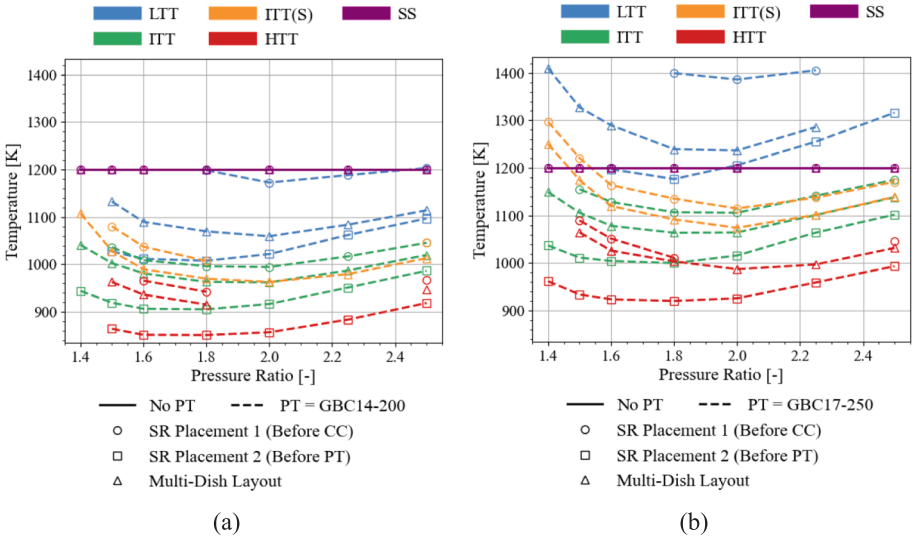

Fig. 16. GT inlet temperature as a function of pressure ratio for various parallel-flow and single-shaft single-dish and multi-dish recuperated solar cycle configurations with (a) the GBC14-200 as the PT and (b) the GBC17-250 as the PT. Note that the single-dish results were reproduced from Refs. [25,26] for comparison purposes.

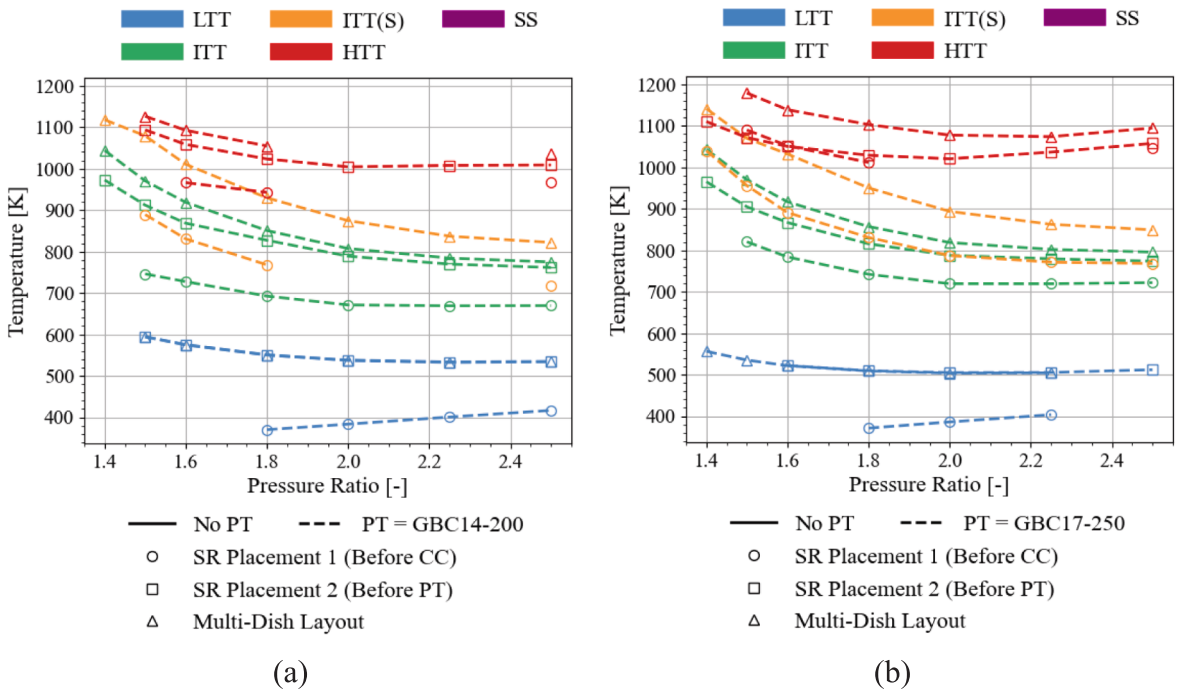

Fig. 17. PT inlet temperature as a function of pressure ratio for various parallel-flow and single-shaft single-dish and multi-dish recuperated solar cycle configurations with (a) the GBC14-200 as the PT and (b) the GBC17-250 as the PT. Note that the single-dish results were reproduced from Refs. [25,26] for comparison purposes.

only operable at pressure ratios greater than 1.64, the multi-dish ITT(S) cycle is only operable at pressure ratios greater than 1.89, and the multi-dish HTT cycle is not operable. However, considering the high gasifier turbine inlet temperatures of some of these cycles with the GBC17-250 power turbine (as discussed using Fig. 16(b)), the multi-dish LTT cycle is not operable for any of the simulated pressure ratios. The remaining multi-dish cycle operational pressure ratio range limitations, caused by high gasifier turbine inlet temperatures, occur at pressure ratios that are already excluded by the high solar receiver surface temperatures and thus do not further limit the pressure ratio ranges of the cycles.

3.2.3. Solar receiver efficiency and recuperator effectiveness

For the efficiencies of the various solar receivers in each of the multi-dish cycles, Fig. 19 shows that the multi-dish LTT cycle, with both power turbine options, has the highest solar receiver efficiencies in the second receiver, which is approximately the same as the receiver efficiencies obtained for the respective LTT (SR-PT) cycles, for the entire pressure ratio range, in comparison to all the other multi-dish solar receiver efficiencies. The multi-dish LTT cycle does have the lowest parallel-flow solar receiver efficiencies for the first solar receiver. However, these low solar receiver efficiencies, in the first receiver of the multi-dish LTT cycles, are higher than all the solar receiver efficiencies in the multi-dish single-shaft cycle, except for at pressure ratios of approximately less than 1.55 for the GBC14-200 power turbine and 1.57 for the GBC17-250 power turbine. Additionally, the multi-dish LTT cycles are shown to have considerably higher solar receiver efficiencies than their respective LTT (SR-CC) cycles. This is due to a lower mass flow rate being required to operate the power turbine when there is a higher power turbine inlet temperature (as caused by the second solar receiver in the multi-dish setup). This lower mass flow rate means that a greater proportion of mass flows through the first solar receiver which improves the efficiency of the first solar receiver.

Moreover, Fig. 20 shows that the multi-dish LTT cycle obtains the highest recuperator effectiveness values, at each pressure ratio, out of the parallel-flow cycles with the GBC14-200 as the power turbine. This excludes the LTT (SR-CC) cycle which only obtains solutions at pressure ratios between 1.8 and 2.5, where lower recuperator effectiveness values are obtained due to the recuperator effectiveness decreasing with an increase in the pressure ratio. When the GBC17-250 is used as the power turbine, higher overall recuperator effectiveness values are obtained, but it has been discussed, in Section 3.2.2, that many of these cycles have high gasifier turbine inlet temperatures, power turbine inlet temperatures, and/or maximum solar receiver surface temperatures when the GBC17-250 is used as the power turbine. This is particularly observed in the multi-dish LTT and LTT (SR-CC) cycles with the GBC17-250 as the power turbine due to the selection of poor performing recuperator geometries to obtain solutions within, or closer to, the temperature limits.

The multi-dish single-shaft cycle performs worse than the single-dish single-shaft cycle in terms of recuperator effectiveness values. These single-dish and multi-dish single-shaft cycles offer the lowest recuperator effectiveness values out of all the cycles (except for the multi-dish LTT and LTT (SR-CC) cycles with the GBC17-250 as the power turbine). This is due to not obtaining solutions for a greater number of recuperator channels (as shown in Appendix B). The combination of the high solar receiver efficiencies and high recuperator effectiveness values results in the high thermal efficiencies in the multi-dish LTT cycle with the GBC14-200 as the power turbine.

4. Conclusion

In conclusion, various multi-dish single-shaft and parallel-flow configurations have been simulated, with the G25-550 (AR = 0.92) as the main shaft turbocharger, and the GBC14-200 and the GBC17-250 as power turbine options in the various parallel-flow cycles. This was done to determine whether a multi-dish cycle, in various unrecuperated and recuperated solar cycle setups, offers a feasible thermal efficiency improvement over its single-dish solar cycle counterparts, which have been simulated in previous studies. An analytical approach has been followed to solve the various cycle configurations so that conclusions can be made regarding cycle efficiency.

For a unrecuperated solar cycle, a multi-dish setup does not offer

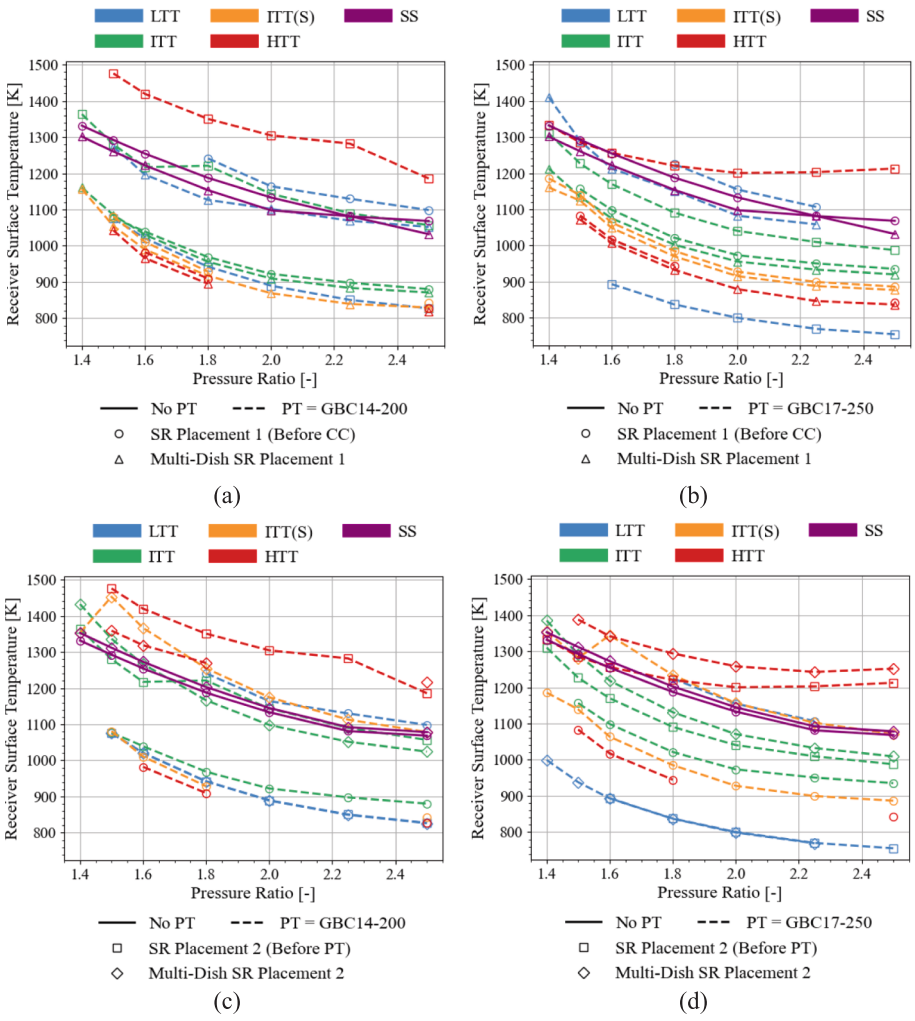

Fig. 18. Maximum solar receiver surface temperature as a function of pressure ratio for various parallel-flow and single-shaft single-dish and multi-dish recuperated solar cycle configurations with (a) the GBC14-200 as the PT with SR placement 1, (b) the GBC17-250 as the PT with SR placement 1, (c) the GBC14-200 as the PT with SR placement 2, (d) and the GBC17-250 as the PT with SR placement 2. Note that the single-dish results were reproduced from Refs. [25,26] for comparison purposes.

great thermal efficiency improvements (for all the considered single-shaft and parallel-flow cycle configurations). Thus it may not be warranted to implement an unrecuperated multi-dish setup due to the additional capital expenditure associated with manufacturing a multi-dish cycle, as this would involve manufacturing two solar dishes and receivers instead of a single dish-receiver setup. However, a detailed cost analysis would be required to confirm this. This is as a result of the thermal efficiency improving by only 5.9 % with a reduction of 3.8 % in power output, when comparing the maximum thermal efficiency results of the multi-dish single-shaft cycle with reference to the single-dish single-shaft cycle. This is a slight improvement over the single-dish single-shaft cycle but additional components would be required to obtain the bigger dish-size, which reduces the viability of a multi-dish unrecuperated solar single-shaft cycle. The single-shaft cycles offer much better thermal efficiency and power output performance than the parallel-flow cycles in an unrecuperated solar cycle setup, which is why these cycles have been used as the metric of comparison. However, the parallel-flow cycles do not experience a loss in power output when incorporating a multi-dish set-up which adds to the viability of a multi-dish unrecuperated solar parallel-flow cycle, but these cycles still do not offer overall better cycle performance.

In a recuperated solar cycle, the addition of a second solar receiver allows for a great improvement in thermal efficiency in the multi-dish LTT configuration, when the G25-550 (AR = 0.92) is used as the main shaft turbocharger. When the multi-dish LTT cycle is configurated with the GBC14-200 as the power turbine, the cycle achieves a thermal efficiency of 39.6 % at a pressure ratio of 1.6, with a power output of 2.5 kW, without exceeding any of the temperature restrictions. This is the highest thermal efficiency obtained out of all the considered cycles, in the current study.

The configuration that obtains the second-highest thermal efficiency in the current study is the single-dish recuperated LTT cycle with the

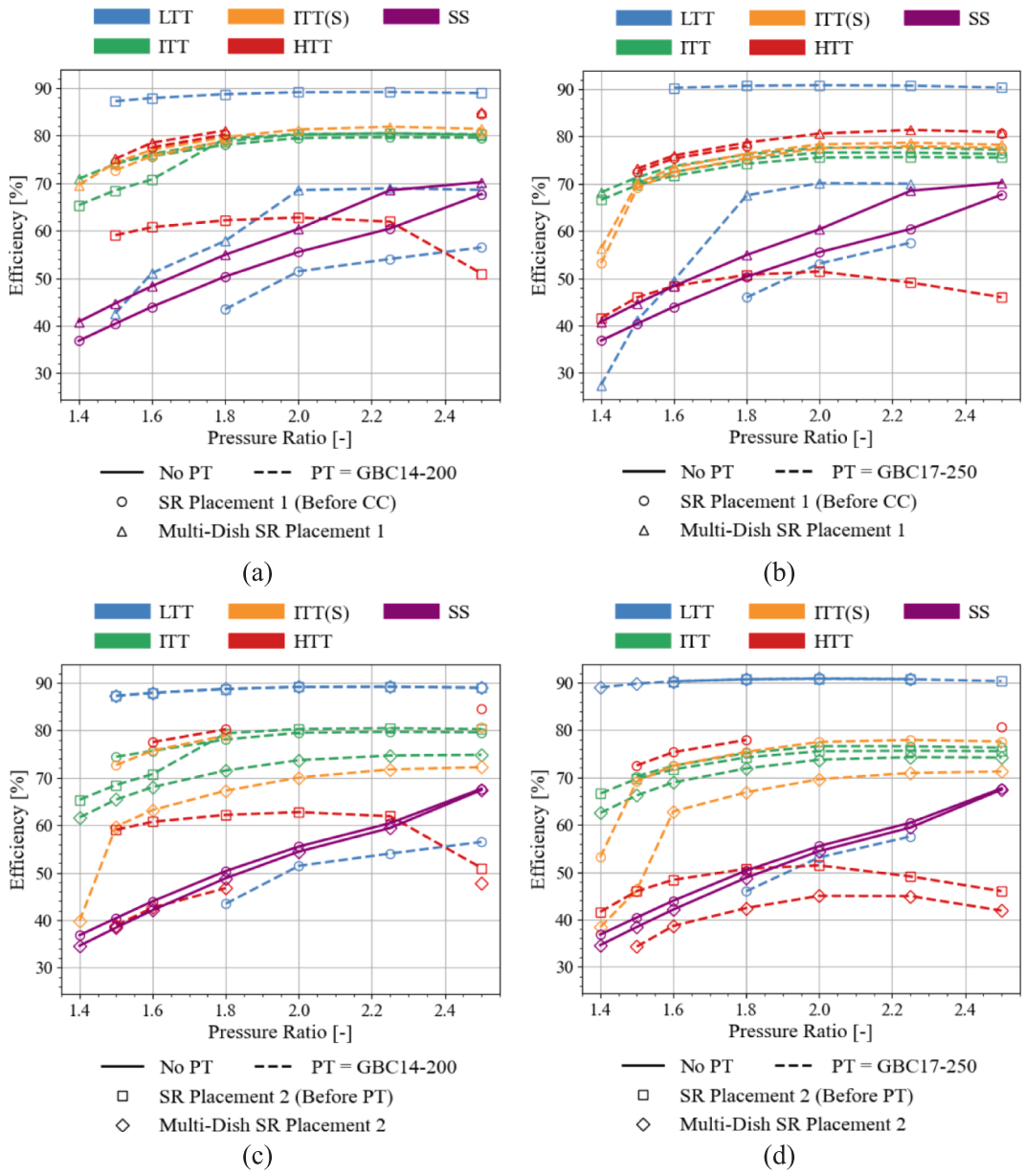

Fig. 19. Solar receiver efficiency as a function of pressure ratio for various parallel-flow and single-shaft single-dish and multi-dish unrecuperated solar cycle configurations with (a) the GBC14-200 as the PT with SR placement 1, (b) the GBC17-250 as the PT with SR placement 1, (c) the GBC14-200 as the PT with SR placement 2, (d) and the GBC17-250 as the PT with SR placement 2. Note that the single-dish results were reproduced from Refs. [25,26] for comparison purposes.

solar receiver prior to the power turbine inlet and with the GBC17-250 as the power turbine, with a thermal efficiency of 23.5 % and a power output of 3 kW at a pressure ratio of 1.6. Thus, the recuperated multi-dish LTT cycle with the GBC14-200 as the power turbine offers a percentage improvement in thermal efficiency of 68.5 % over the recuperated single-dish LTT cycle with the GBC17-250 power turbine and with power turbine placed before the power turbine inlet. This higher thermal efficiency is expected to reduce the cycle running costs due to having a higher power output with reference to the fuel that is added to the cycle.

Both the recuperated multi-dish LTT cycle with the GBC14-200 as the power turbine and the recuperated LTT cycle with a single solar receiver prior to the power turbine inlet and with the GBC17-250 as the power turbine offer better feasible thermal efficiency results than the single-dish and multi-dish single-shaft cycles. The recuperated solar single-dish single-shaft cycle has a maximum feasible thermal efficiency of 21.8 % with a power output of 4.6 kW at a pressure ratio of 1.75, due to cycle restrictions caused by high solar receiver surface temperatures. Considering the maximum solar receiver surface temperature restrictions, the recuperated solar multi-dish single-shaft cycle obtains a thermal efficiency of 21.1 % with a power output of 4.2 kW at a pressure ratio of 1.81. This is an important finding as the recuperated multi-dish

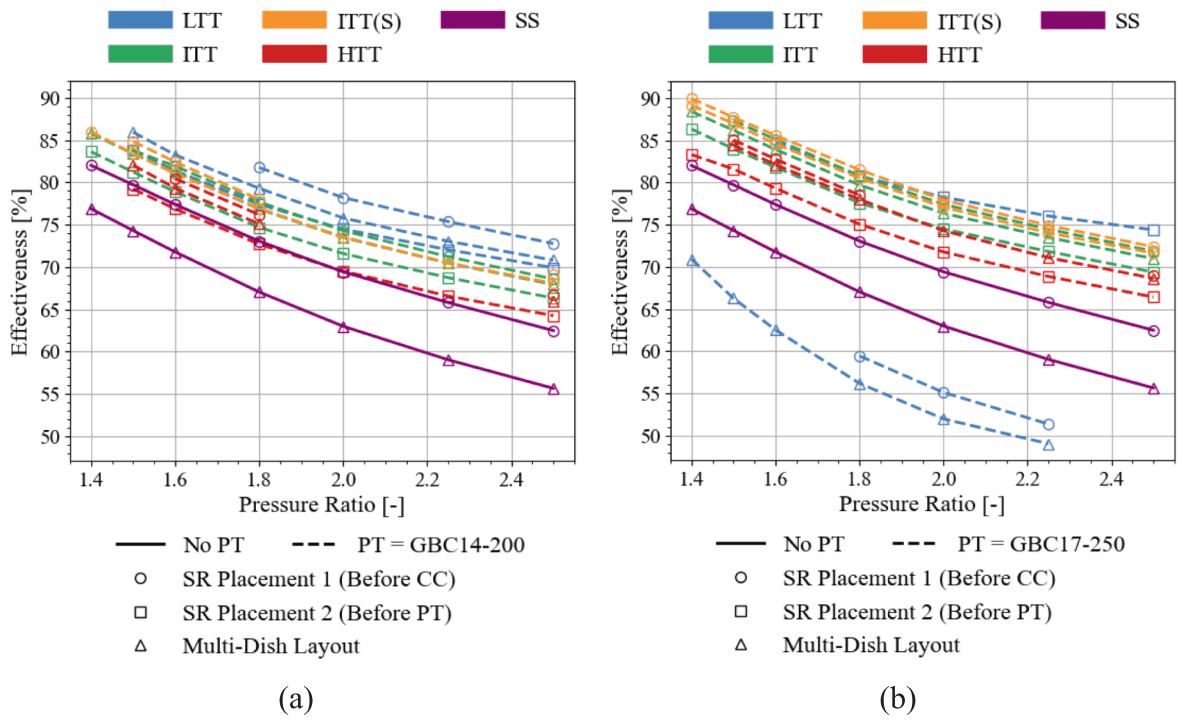

Fig. 20. Recuperator effectiveness as a function of pressure ratio for various parallel-flow and single-shaft single-dish and multi-dish recuperated solar cycle configurations with (a) the GBC14-200 as the PT and (b) the GBC17-250 as the PT. Note that the single-dish results were reproduced from Refs. [25,26] for comparison purposes.

parallel-flow LTT cycle with the GBC14-200 as the power turbine is operable at lower pressure ratios for better solar heat capture than in the multi-dish single-shaft cycle. Thus, when the multi-dish setup is combined with a parallel-flow configuration (specifically the recuperated LTT configuration), the receiver is operable at lower temperatures than in a single-shaft setup. This better solar heat capture allows for greater cycle efficiencies in the recuperated parallel-flow LTT cycle due to remaining within the specified solar receiver surface temperature limit. This is however not true for single-shaft cycles which means the extra cost of implementing a multi-dish cycle would have to be carefully considered in future work. Note that, the solar receiver temperature constraint in the current study can however be overcome by using other materials, as can also be investigated in future studies.

4.1. Recommendations

Overall, to obtain the maximum cycle thermal efficiency for reducing the running costs (saving fuel) associated with heating the cycle, it is recommended to implement the recuperated solar multi-dish LTT cycle with the GBC14-200 as the power turbine. However, this multi-dish setup requires higher initial capital expenditure due to requiring two solar receivers and a bigger dish to achieve the required setup. Thus, for obtaining the highest thermal efficiency without implementing a multi-dish setup, the LTT cycle with the GBC17-250 as the power turbine offers the highest feasible thermal efficiency under the consideration of a combustion chamber pressure loss of 6 %. This specifically applies to the placement of the solar dish prior to the power turbine inlet. Both of these cycles obtain their highest feasible thermal efficiencies at a compressor pressure ratio of 1.6. This low pressure ratio operation is further recommended due to allowing for a longer lifespan for the cycle components due to not subjecting the components to excessively high pressures. This is further beneficial for continuous cycle operation.

To further expand upon the current study, it is recommended to further analyse the solar receiver and solar dish geometry, with a consideration of how the SolTrace ray tracing differs with different solar component structures, to ascertain whether the solar receiver and dish setups in the current study allow for maximum cycle performance. The multi-dish single-shaft cycle structures can also be considered in terms of the placement of the solar receivers in parallel rather than in series. Additionally, a concept of splitting the solar heat with a single-dish can be investigated under the consideration that a single-receiver is utilised with the receiver coils being split into a top part of the receiver and a bottom part of the receiver. Each of these receiver parts would have its own inlet and its own outlet to distribute the solar heat to their various cycle locations. This split receiver concept would need to be investigated further for technical feasibility. A cost analysis can also be done to determine the timespan in which the operation of a multi-dish setup warrants the initial additional costs associated with the manufacturing of a multi-dish cycle in comparison to a single-dish cycle. This can be done via considering the localised cost of energy of the individual cycles. The analysis would also have to extend beyond steady-state assumptions and the assumption of a constant DNI of 1000 W/m^2. A transient study which allows for the intermittency of the sun in a typical year at specific locations would have to be incorporated for a proper feasibility study with cost comparisons. This would need to be done in future work regarding the various cycles.

Lastly, an additional analysis can be implemented regarding utilising the high exergy exhaust gas from the gasifier turbine to heat the power turbine inlet in a recuperation process instead of adding heat to the gasifier turbine flow path of the cycle. This alternative use of the recuperator would introduce additional pressure losses that would reduce the pressure ratio through the power turbine. Thus, a study can be done regarding whether this is a feasible concept for the various multi-dish parallel-flow cycles.

CRediT authorship contribution statement

C.C. Cockcroft: Writing – review & editing, Writing – original draft, Visualization, Software, Methodology, Investigation, Formal analysis, Data curation, Conceptualization. **W.G. Le Roux:** Writing – review &

editing, Writing – original draft, Supervision, Methodology, Funding acquisition, Conceptualization.

Declaration of competing interest

The authors declare that they have no known competing financial interests or personal relationships that could have appeared to influence the work reported in this paper.

Acknowledgements

The authors would like to extend their gratitude to the Department of Science, Technology and Innovation (DSTI), South Africa, for supporting the UP Solar Thermal Spoke through the Renewable Energy Hub and Spokes Programme.

Appendix A. Solution procedures

The various solution procedures for the cycles are shown in Figs. A1 to A4. These procedures are followed to obtain the results in Section 3, through using the procedures detailed in Section 2.2 as well as in the studies by Cockcroft & Le Roux [24,25,26,29]. These procedures consist of the calculations required to determine the temperatures and pressures associated with each component in the respective cycles as well as the steady-state operating point of the turbomachinery. Note that only the solution procedures for the multi-dish LTT cycles are shown in Figs. A1 and A3 to remain succinct (to solve for the remaining parallel-flow cycles, the mass flow rates and state numbers change as per the layouts in Section 2.1, as in the study by Cockcroft & Le Roux [25]). Note that Figs. A1 to A4 show the iteration procedures for each cycle that are followed for each specified pressure ratio as well as for the input recuperator variable geometry options. Additionally, Figs. A2 and A4 only contain one while loop as a result of the combustion outlet temperature being specified as 1200 K as stated in Section 2.2.2.

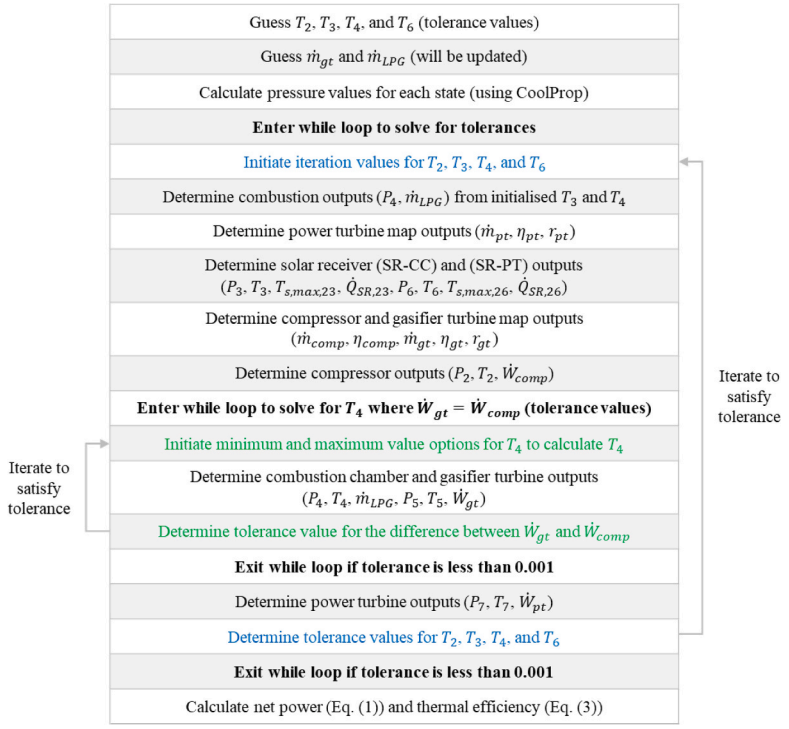

Fig. A1. Unrecuperated solar multi-dish LTT solution procedure (solution to cycle in Fig. 4).

Moreover, the difference between the initiated value and the calculated value of the respective variables in each iteration procedure forms the tolerance required to determine whether the loop conditions are satisfied. Overall, each while loop is terminated when all of its tolerance values fall within a value of no greater than 0.001. This value is chosen to ensure accurate solution procedures while maintaining reasonable computational time.

The procedure occurring in the inner nested while loop is used to determine the required combustion outlet temperature (only in Fig. A1 and Fig. A3 – for the parallel flow cycles). Note that an iterative procedure is used. This is necessary due to the complexity of the combustion function (using enthalpy of formation). In the parallel-flow cycles, the gasifier turbine power needs to equate to the compressor power. Thus, the combustion chamber outlet temperature needs to be a specific value to allow for the compressor power and the gasifier turbine power to be equal to one another. To determine this, the minimum and maximum bounds are initially specified. The combustion outlet temperature may not be lower than the combustion inlet temperature (as the minimum bound). Also, the combustion outlet temperature may not be higher than the maximum flame temperature of the fuel (as the maximum bound). Thus, the combustion outlet temperature should fall between these values.

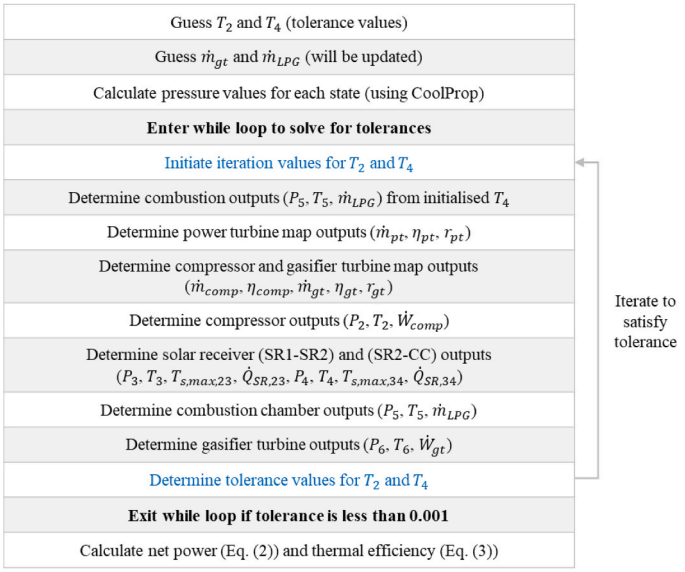

Fig. A2. Unrecuperated solar multi-dish single-shaft solution procedure (solution to cycle in Fig. 5).

For the combustion outlet temperature iteration procedure, the minimum combustion outlet temperature limit and the maximum combustion outlet temperature limit are averaged to determine a third temperature set. Each temperature is then used to determine the required LPG mass flow rate (or air–fuel ratio) to obtain each respective combustion outlet temperature. These values are then used to determine their respective gasifier turbine outputs, including the power generation of the gasifier turbine, thus forming a range of power generation values for each combustion outlet temperature. The required compressor power should fall either between the gasifier turbine power generation calculated via the minimum and average combustion outlet temperatures, or between the gasifier turbine power generation calculated via the average and maximum combustion outlet temperatures. For each option, the maximum and minimum values are adjusted accordingly for the next iteration. This procedure is repeated for every iteration of the while loop until the difference between the compressor power required and the gasifier turbine power generated meets the specified tolerance. When this occurs, the average value is taken as the combustion outlet temperature as the tolerance is met.

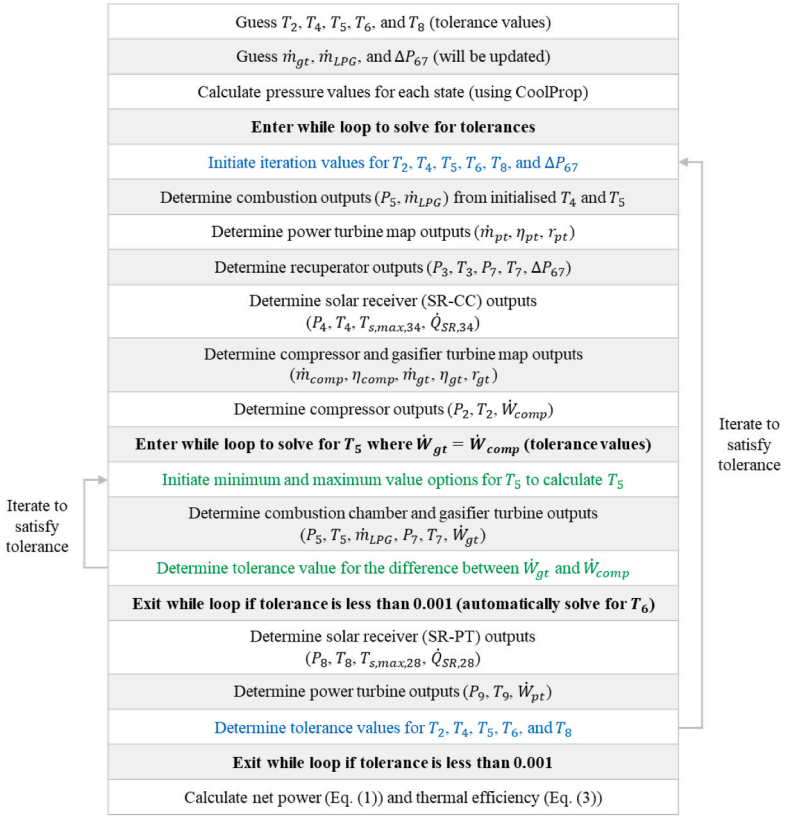

Fig. A3. Recuperated solar multi-dish LTT solution procedure (solution to cycle in Fig. 6).

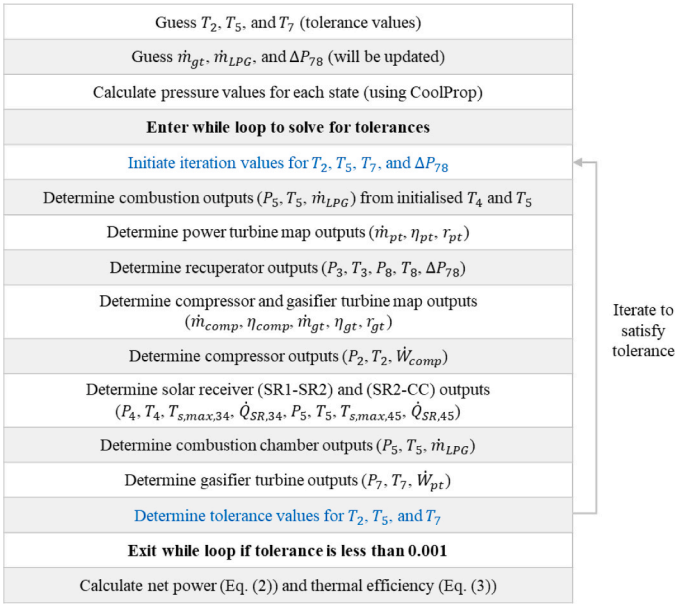

Fig. A4. Recuperated solar multi-dish single-shaft solution procedure (solution to cycle in Fig. 7).

Appendix B. Best recuperator dimensions for each multi-dish recuperated solar configuration

The recuperator dimensions used to generate the recuperated solar multi-dish configuration results are listed in Table B1. These recuperator dimensions are deemed the best recuperator dimensions for the multi-dish cycles, with the best recuperator dimensions for the best single-dish configurations being determined and listed in the studies by Cockcroft & Le Roux [25,26]. The methodology for determining the best-case recuperator dimensions for each multi-dish configuration follows the same procedure as in the reference studies.

Table B1
Recuperator dimensions for each recuperated solar cycle multi-dish configuration for different PT options considering the entire pressure ratio range.

Power Turbine	Cycle Configuration	Number of Channels [-]	Channel Height [mm]
–	SS	22.5	4.50
GBC14-200	LTT	45.0	3.00
	ITT	45.0	2.25
	ITT(S)	45.0	3.75
	HTT	45.0	3.00
GBC17-250	LTT	15.0	3.75
	ITT	45.0	2.25
	ITT(S)	45.0	2.25
	HTT	45.0	3.00

Data availability

Data will be made available on request.

References

[1] Zeb K, Ali SM, Khan B, Mehmood CA, Tareen N, Din W, et al. A survey on waste heat recovery: Electric power generation and potential prospects within Pakistan. Renew Sustain Energy Rev 2017;75:1142–55.
[2] Guo H, Zhang Y, Xu Y, Zhou X, Chen H. Derived energy storage systems from Brayton cycle. iScience 2024;27(4).
[3] Jansen E, Bello-Ochende T, Meyer JP. Integrated solar thermal Brayton cycles with either one or two regenerative heat exchangers for maximum power output. Energy 2015;86:737–48.
[4] García-Ferrero J, Merchán RP, Santos MJ, Medina A, Calvo Hernández A. Brayton technology for concentrated solar power plants: comparative analysis of central tower plants and parabolic dish farms. Energy Conv. Manage. 2022;271.
[5] Wang K, Wan X, Liu J-K, Rao Z-H, Fan Y-H, Min C-H. Thermo-economic analysis and optimization of a novel solar power tower with a cascade supercritical CO2 Brayton cycle for expanding the temperature range of thermal storage. Appl Therm Eng 2025;278. https://doi.org/10.1016/j.applthermaleng.2025.127338.
[6] Sanders Associates Inc. Parabolic dish module experiment. Final test report. New Hampshire, USA: Nashua; 1986.
[7] Garrett Turbine Engine Co., "Brayton cycle solarized advanced gas turbine: Final report," Phoenix, Arizona, USA, DOE/NASA/0181, 1986.
[8] Jaffe LD. Test results on parabolic dish concentrators for solar thermal power systems. Sol Energy 1989;42(2):173–87.
[9] Lanchi M, Montecchi M, Crescenzi T, Mele D, Miliozzi A, Russo V, et al. Investigation into the coupling of micro gas turbines with CSP technology: OMSoP project. Energy Procedia 2015;69:1317–26.
[10] Lanchi M, Al-Zaili J, Russo V, Falchetta M, Montecchi M, Aichmayer L. A quasi-steady state model of a solar parabolic dish micro gas turbine demonstration plant. Energies 2022;15(3).
[11] Kesseli J, Vollnogle E. "Brayton Power Conversion System," Brayton Energy LLC, DE-FC36-08GO18029/A000. New Hampshire, USA: Hampton; 2011.
[12] Sammoutos C, Kitsopoulou A, Lykas P, Bellos E, Tzivanidis C. Dynamic investigation of a solar-driven brayton cycle with supercritical CO2. Appl Syst Innov 2023;6(71).
[13] Le Roux WG, Bello-Ochende T, Meyer JP. The efficiency of an open-cavity tubular solar receiver for a small-scale solar thermal Brayton cycle. Energ Conver Manage 2014;84:457–70.

[14] WG Le Roux, JP Meyer, "Modeling the Small-Scale Dish-Mounted Solar Thermal Brayton Cycle," in AIP Conference Proceedings, Vol. 1734, No. 1, AIP Publishing, 2016. https://doi.org/10.1063/1.4949144.
[15] WG Le Roux, "Feasibility study of a hybrid small-scale dish-mounted solar thermal Brayton cycle with cogeneration," in *International Heat Transfer Conference*, 2018, 10-15 August, pp. 7929–7936. https://doi.org/10.1615/IHTC16.nee.0241.
[16] Le Roux WG, Sciacovelli A. Recuperated solar-dish Brayton cycle using turbocharger and short-term thermal storage. Sol Energy 2019;194(2019):569–80.
[17] Humbert G, Roosendaal C, Swanepoel JK, Navarro HM, Le Roux W, Sciacovelli A. Development of a latent heat thermal energy storage unit for the exhaust of a recuperated solar-dish Brayton cycle. Appl Therm Eng 2022;216:1–15.
[18] Swanepoel JK, Le Roux WG, Roosendaal C, Madani SH, De Wet G, Nikolaidis T, et al. Initial experimental testing of a hybrid solar-dish Brayton cycle for combined heat and power (ST-CHP). Appl Therm Eng 2024;249:1–22.
[19] Van der Merwe AH, Le Roux WG, Humphries ED. Parallel turbochargers for small-scale power generation. Appl Therm Eng 2023;235:1–23.
[20] De Beer JH, Le Roux WG, Sciacovelli A, Meyer JP. Effect of a novel cooling window on a recuperated solar-dish Brayton cycle. Renew Energy 2023;208(7):465–80.
[21] Butt MU. "Converting an automobile turbocharger into a micro gas turbine," in the 3rd International Conference on Power, Energy and Mechanical Engineering (ICPEME 2019). Prague: Czech Republic; 2019.
[22] Visser WPJ, Shakariyants SA, Oostveen M. Development of a 3 kW microturbine for CHP applications. J Eng Gas Turbines Power 2011;133(4):1–8.
[23] Akba T, Baker DK, Pınar Mengüç M. Off-design performance of micro-scale solar Brayton cycle. Energy Conv Manage 2023;289.
[24] Cockcroft CC, Le Roux WG. A comparative analysis between small-scale recuperated parallel-flow Brayton cycles. Appl Therm Eng 2025;267.
[25] Cockcroft CC, Le Roux WG. The influence of applying a solar-dish to parallel-flow configurations of a Brayton cycle. Sol Energy 2025;288.
[26] Cockcroft CC, Le Roux WG. A comparative overview of various single-shaft and parallel-flow Brayton cycles developed from turbochargers. Energ Conver Manage 2025;335.
[27] Brun K, Friedman P, Dennis R. Fundamentals and applications of Supercritical Carbon Dioxide (SCO2) based Power Cycles. Woodhead Publishing 2017.
[28] Zhu Y, Zhai R, Yang Y, Reyes Belmonte M. Techno-economic analysis of solar tower aided coal-fired power generation system. Energies 2017;10.
[29] Cockcroft CC, Le Roux WG. The influence of applying turbine inlet air cooling to a small-scale parallel-flow Brayton cycle. Energ Conver Manage 2025;325.
[30] Automeris, "Extract data from charts," 2024. [Online]. Available: https://automeris.io/. [Accessed 2 August 2024].
[31] Garrett Motion, "Garrett Performance Turbo," 2023. [Online]. Available: https://www.garrettmotion.com/racing-and-performance/performance-turbos/?term_id=28. [Accessed 11 May 2023].
[32] Garrett Motion, "GARRETT G42-1200 73MM," 2024. [Online]. Available: https://www.garrettmotion.com/racing-and-performance/performance-catalog/turbo/g-series-g42-1200/. [Accessed 2 August 2024].
[33] Rankokwane B, Makhurutha SE, Makhurutha T, Motlasuping T. Liquefied petroleum gas market study. Lobatse: Botswana Energy Regulatory Authority; 2021.
[34] Lefebvre H, Ballal DR. Gas Turbine Combustion: Alternative Fuels and Emissions. 3rd ed. Boca Raton: Taylor and Francis Group, LLC; 2010.
[35] Nellis GF, Pfotenhauer JM. Effectiveness-NTU relationship for a counterflow heat exchanger subjected to an external heat transfer. J Heat Transfer 2005;127:1071–3.
[36] The National Renewable Energy Laboratory, "SolTrace," [Online]. Available: https://www.nrel.gov/csp/soltrace.html. [Accessed 20 August 2024].